J Ther Eng, Vol. 11, No. 4, pp. 1193−1230, July, 2025

Journal of Thermal Engineering
Web page info: https://jten.yildiz.edu.tr
DOI: 10.14744/thermal.0000972

Review Article

# Advances in passive heat transfer enhancement for heat exchangers: a comprehensive review

**Muhammad Ali KHAN[1], Muhammad ILYAS[1], Khalid WAHEED[1], Inamul HAQ[1], Fatih AYDOGAN[2]**

*[1]Department of Nuclear Engineering, Pakistan Institute of Engineering and Applied Sciences, Islamabad, 04403, Pakistan*
*[2]Jacksonville University, Florida, 32211, USA*

## ARTICLE INFO

*Article history*
Received: 06 October 2024
Revised: 07 October 2024
Accepted: 31 October 2024

**Keywords:**
Air Bubble Injection; Extended Surfaces; Heat Transfer Enhancement; Micro-Surfaces; Nanofluids; Passive Methods; Phase Change Materials; Printed Circuit Heat Exchangers; Tape Inserts; Vortex Generators

## ABSTRACT

This paper reviews the latest advances in passive heat transfer enhancement techniques, addressing the gap in the literature regarding recent developments. Heat exchangers are crucial in improving energy efficiency in various industrial applications, including power plants and nuclear reactors. Various heat enhancement techniques such as geometric modifications, air bubble injection, vortex generators, tape inserts, micro-surfaces, baffles, printed circuit heat exchangers, and phase change materials are studied. These techniques are evaluated based on heat transfer rate, pressure drop, and performance evaluation criteria. It is found from this review that the air bubble injection in shell and tube heat exchangers demonstrates the highest performance evaluation criteria of 4.5. However, its application is limited by process constraints. On the other hand, the Y-shaped tape inserts with a trapezoidal configuration though having a slightly lower performance evaluation criteria of 3.68 is easier to implement in existing and new designs. In printed circuit heat exchangers, zigzag channels exhibit a 50% improvement in thermal performance compared to straight channels. The study also highlights the potential of gyroid structures for application in high-pressure and high-temperature systems, such as advanced nuclear reactors. The comprehensive evaluation of heat enhancement techniques provides designers and engineers with a practical insight into designing heat exchanger for specific system requirements.

**Cite this article as:** Khan MA, Ilyas M, Waheed K, Haq I, Aydogan F. Advances in passive heat transfer enhancement for heat exchangers: a comprehensive review. J Ther Eng 2025;11(4):1193−1230.

## INTRODUCTION

The primary objective of a power plant is to convert thermal energy into mechanical energy for electricity generation. Heat transfer is an essential process that has a direct impact on the plant's efficiency and environmental sustainability. However, achieving high-efficiency energy conversion faces challenges due to inherent limitations in heat transfer processes, particularly due to boundary layer formation. This

***Corresponding author.**
*E-mail address: faydogan@gmail.com

*This paper was recommended for publication in revised form by Editor-in-Chief Ahmet Selim Dalkılıç*

phenomenon establishes the existence of a laminar sub-layer with minimal fluid velocity in the heat exchanger (HX) tubes [1, 2]. The stagnant layer, dominated by thermal conduction, acts as a primary resistance to heat transfer, emphasizing the need for innovative techniques [3].

Efficient heat transfer is crucial for power generation and the longevity of industrial systems, ranging from power plants to electronic cooling [4]. Traditional HXs often face limitations in achieving optimal heat transfer rates, leading to increased energy consumption and reduced system efficiency. Exploring advanced techniques becomes imperative to address these challenges and develop sustainable and energy-efficient technologies [5]. Optimization of the heat exchange process remains an active area of research across various engineering applications.

HXs are essential components in many industrial processes facilitating thermal energy transfer between two fluids without direct contact [6]. Their applications span a wide range of industries, including power generation [7], chemical processing [8], HVAC [9], automotive [10], and aerospace [11]. The widespread use of HXs has driven researchers towards technological advancements and innovative designs. These advancements focus on improving the heat transfer coefficient while minimizing pressure drop, which leads to higher efficiency and more compact equipment. Energy-efficient HXs play a key role in reducing energy consumption, lowering operational costs, and minimizing environmental impact. In critical applications such as nuclear reactors and advanced manufacturing, HXs are crucial for maintaining safe and stable operating conditions, increasing their significance in modern industrial systems.

A lot of review papers are available on heat transfer enhancement techniques, with some focusing specifically on concentric tube [12-14] and plate type HXs [15], while others cover single phase [16, 17], two-phase [18] and phase change materials [19]. Some researchers examine specific heat enhancement techniques such as dimple surface [20], insert and nanofluid [21], porous media [22], extended surfaces [23], twisted tape [24-26], micro surface modification [27], swirl flow devices [28], nanosuspension [29] and microchannel heat sink [30]. Some reviewers also summarize various passive techniques [31, 32], active techniques [33, 34], and combined passive and active techniques [35-37]. The motivation for the present review paper stems from the fact that the available review papers lack the inclusion of the most recent developments across the entire spectrum of heat transfer enhancement techniques. It is thus required to conduct a comprehensive and up-to-date review of the different heat enhancement techniques.

This review focuses on classifying and analyzing the latest research on passive heat enhancement techniques, thereby offering insights into their applications in the next generation of HXs. The review covers a range of HX configurations, from traditional tubular designs to cutting-edge micro-channel HXs, characterizing them based on heat transfer rate, pressure drop, and performance evaluation criteria (PEC). It contributes to the understanding of heat enhancement using geometric parameters, air bubble injection, vortex generators, tape inserts, micro-surfaces, and baffles in tubular HX, as well as straight, zigzag, and airfoil channels in printed circuit heat exchangers (PCHE) and phase change materials. The innovative techniques supported by pictorial representations highlighting their salient features are summarized in tables.

This review serves as a valuable resource for designers and engineers looking to develop HX designs tailored to specific system requirements. By presenting the advantages and limitations of various heat transfer enhancement techniques, the review facilitates the selection of the most suitable configurations for the development of more efficient, cost-effective, and sustainable HX designs.

**Heat Enhancement Using Geometric Parameters**

In this section, the heat transfer characteristics improved by changing the geometrical configurations in the tubular HX are reviewed. This approach focuses on optimizing the surface area and flow patterns within the HX to enhance heat transfer rates. Tubular HXs are the most important part of the power plant and process industry, where effective heat transfer is essential for achieving desired operational outcomes. The shell and tube and the double pipe HXs are the most commonly used heat transfer equipment in the industry [38]. However, these types of HX require large spaces and are less efficient in heat transfer. To address these limitations, a lot of researchers are working on new types of HXs that are compact, efficient, and easy to maintain as summarized in Table 1.

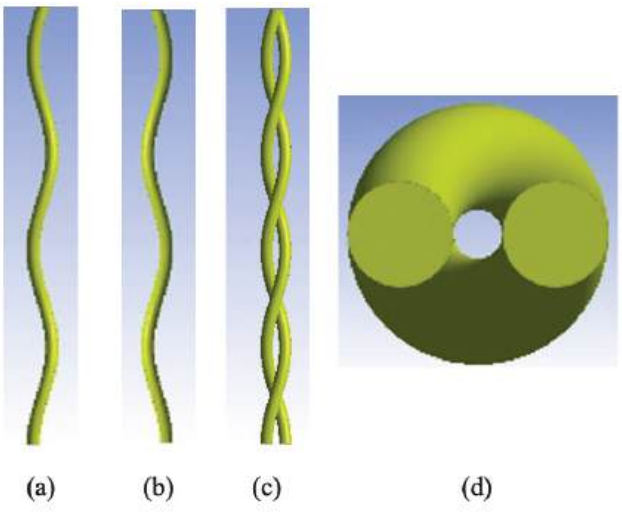


**Figure 1.** A single module of twined tube HX: (a) tube-1, (b) tube-2, (c) twined tubes, and (d) top view. [From Khan et al. [39], with permission from Elsevier.]

**Table 1.** Heat enhancement using geometric parameters

| Author | Year | Geometry type | Analysis type | Key findings |
|---|---|---|---|---|
| Khan et al. [39] | 2024 | Twined tube HX | Experimental and computational | The design outperforms straight tube designs, achieving a peak performance improvement of 60%. |
| Li et al. [40] | 2023 | Corrugated tubes | Experimental and computational | Enhances the heat transfer from ice by 30% compared to smooth tubes. |
| Qin et al. [41] | 2023 | Spirally corrugated pipes | Experimental | Convective heat transfer is improved due to increased velocity fluctuations in the pipe, resulting in a higher ΔT. |
| Hu et al. [42] | 2022 | TCT | Experimental and computational | Shows the highest Nu and friction factor compared to OCT and HCT and is 60% larger Nu compared to smooth tubes. |
| | | OCT | | Exhibits the lowest Nu and friction factor compared to TCT and HCT. |
| | | HCT | | Lower friction factor and high Nu show the highest PEC of 1.09 compared to TCT and OCT. |
| Rezaei et al. [43] | 2023 | STST | Computational | With a -30° rotation angle at the tube inlet, the PEC is improved by 11.14%. |
| | | TTST | | The maximum PEC of 1.25 is achieved with 13 twists and a Re of 1000. |
| Khashaei et al. [44] | 2023 | Deep dimpled tubes | Experimental | Is effective within a range from 1000 to 2250 Re range but is less applicable below 1000 Re. The maximum increase in PEC of 2.71 is observed. |
| Xin et al. [45] | 2023 | Eccentric tubes | Computational | At an eccentric tube lead length (s) of 50 mm and eccentric distance (a) of 4 mm, achieves a maximum PEC of 2.43. |
| Li et al. [46] | 2024 | EHTs | Computational | EHTs with a pitch of 25 mm, eccentricity of 1.5 mm, and tube diameter of 6 mm show superior performance for heat transfer enhancement in $sCO_2$ HXs. |
| Zahrani et al. [47] | 2021 | Novel gasket design in a FPHE | Computational | Significantly increases Nu by 70% and friction factor by 3.4 to 4.4 times compared to standard FPHE. |
| Yahiat et al. [48] | 2023 | External and internal wall deformations | Computational | The optimal geometry proposes achieving 81% higher thermo-hydraulic performance and a PEC as high as 3.10 with the smallest pitch at Re of 1000. |

Khan et al. present an innovative twined tube HX design for advanced nuclear reactors (Figure 1). The twined tube HX outperforms straight tube designs, exhibiting a maximum performance enhancement of 60% [39]. Li et al. develop corrugated tube HXs for ice storage and compare their heat transfer characteristics with straight tube HX. During the ice storage process, the heat transfer rate from the corrugated HX is 30% faster compared to the straight tube HX [40]. Qin et al. develop a spirally corrugated pipe (pitch/diameter of 2.22). They study the flow disturbance in the fluid using stereoscopic particle image velocimetry (Figure 2). The result shows that the heated wall and spirally corrugated pipe increase the turbulence in the fluid resulting in a higher temperature difference along the pipe [41]. Hu et al. investigate the three corrugated tube designs as shown in Figure 3. The research shows that corrugation disrupts the formation of the boundary layer and increases fluid mixing. The design improves convective heat transfer and reduces temperature gradients normal to the flow direction. The transversely corrugated tube (TCT), with an e/d (dimensionless height) of 0.03 and a p/d (dimensionless pitch) of 0.6 at a Reynold number (Re) of 20,000, shows a 60% improvement in the Nusselt number (Nu) compared to a smooth tube. The helically corrugated tube (HCT), with the same e/d and p/d values at a Re of 12,000, demonstrates the highest PEC of 1.09 [42].

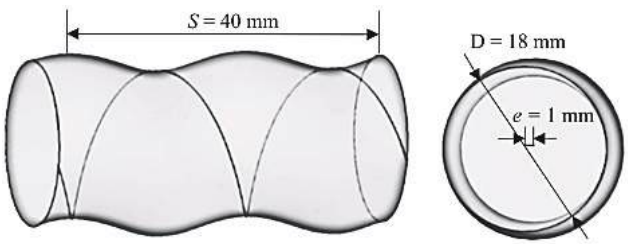


**Figure 2.** Geometrical models of spirally corrugated pipe. [From Qin et al. [41], with permission from Elsevier.]

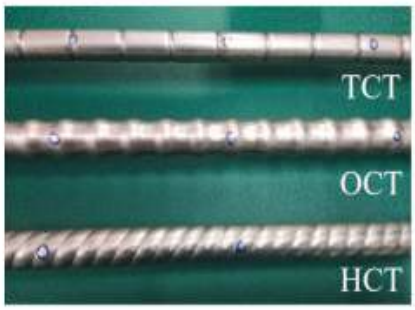


**Figure 3.** Geometrical models of a transversely corrugated tube (TCT), outward corrugated tube (OCT), and helically corrugated tube (HCT). [From Hu et al. [42], with permission from Elsevier.]

Rezaei et al. introduce smooth tri-lobed spiral tubes (STST) and twisted tri-lobed spiral tubes (TTST) HX designs as shown in Figure 4. The authors perform numerical simulations to find the thermohydraulic performance of the designs. The STST with a -30° rotation angle at the tube inlet, enhances PEC by 11.14%, while TTST performance improves with increased twists. The highest PEC value of 1.25 is obtained for TTST with a 1.25 pitch and 13 twists at a Re of 1000 [43]. Khashaei et al. investigate the deep dimpled tubes that enhance mixing in both longitudinal and circumferential directions (Figure 5). Experiments are conducted in a laminar region with constant wall heat flux. The results show a 3.25 times improvement in the convection heat transfer coefficient and maximum PEC of 2.71 as compared to the smooth tube [44].

Xin et al. introduce an eccentric tube design HX to enhance heat transfer performance (Figure 6). The longitudinal vortex structure in the eccentric tube increases the convection heat transfer by reducing the thickness of hydrodynamic and thermal boundary layers through fluid mixing in the boundary and core flow area. The Nu and friction fraction also increase with the increase in the eccentricity. The maximum PEC of 2.43 is achieved at an eccentric tube lead length (s) of 50 mm and eccentric distance (a) of 4 mm [45]. Li et al. propose a novel eccentrical helical tube (EHT) design and perform multiple numerical simulations (Figure 7). An increase in Nu and a decrease in friction factor are observed with the increase in the mass flux of the working fluid ($sCO_2$). An opposite effect is observed in the case of the increase in the fluid pressure and higher heat flux. They also study the geometric parameters and find that a 6 mm tube diameter with a pitch (s) of 25 mm and eccentricity (e) of 1.5 mm shows optimal thermal-hydraulic performance. Moreover, the EHT exhibits superior performance compared to twisted elliptical tube, and conical tube configurations [46].

**Figure 4.** Geometrical models of STST (left) and TTST (right). [From Rezaei et al. [43], with permission from Elsevier.]

**Figure 5.** A three-dimensional view of a tube with deep dimples. [From Khashaei et al. [44], with permission from Elsevier.]

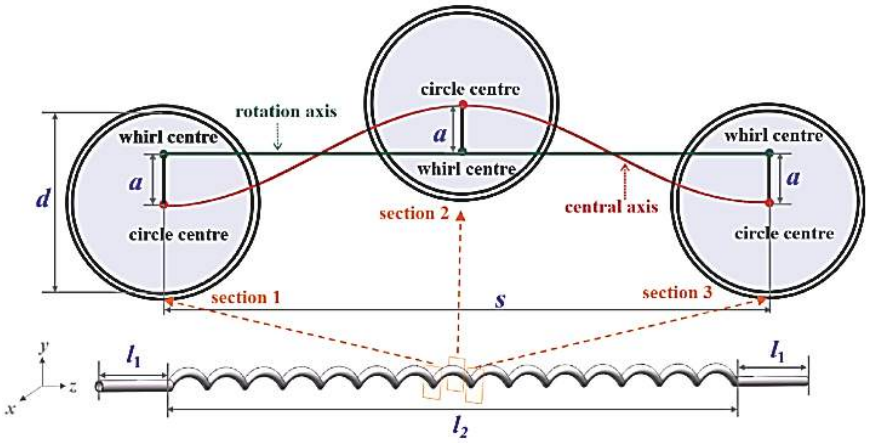


**Figure 6.** Model diagram of an eccentric tube. [From Xin et al. [45], with permission from Elsevier.]

Zahrani et al. present a novel design for the flat plate HX (FPHE), placing both inlet and outlet ports on the same side of the thermal plate. This modification enhances thermal performance, with a 70% increase in Nu and a 3.4 to 4.4 times increase in friction factor compared to the standard FPHE [47]. Yahiat et al. numerically study external and internal wall macro deformations on HX (Figure 8). The wavy external wall deformations generate large-scale longitudinal vortices and transverse secondary flows. The geometries with small pitch values have more intense macro structures, which enhance flow mixing and convection heat transfer. The combination of external and internal macro deformation geometry achieves 81% higher thermo-hydraulic performance. A PEC of 3.10 is achieved with the lowest pitch at Re of 1000 [48].

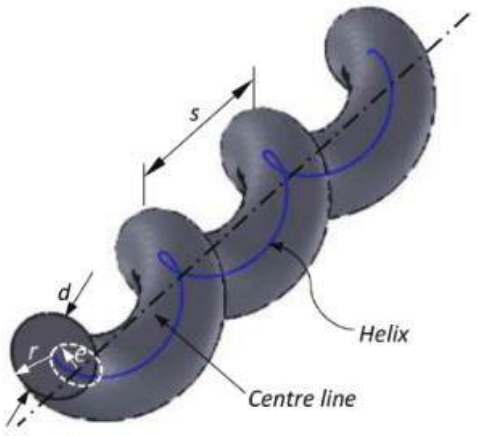


**Figure 7.** EHT HX model diagram. [From Li et al. [46], with permission from Elsevier.]

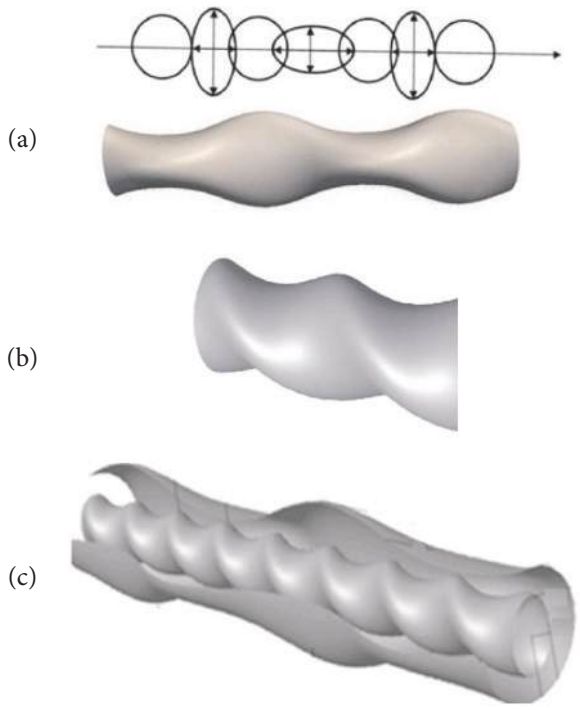


**Figure 8.** Macro wall deformation geometry schemes: (a) external wall deformation, (b) internal wall deformation, and (c) combination of internal and external wall deformation. [From Yahiat et al. [48], with permission from Elsevier.]

**Heat Enhancement Using Air Bubble Injection**

This section explores various methods to enhance heat transfer using turbulators/baffles, air bubble injection, and nanofluids. These techniques involve disrupting the thermal boundary layer and enhancing the thermophysical properties of the fluid by implementing and testing different enhancement methods to determine their individual and combined effects on heat transfer performance. The effectiveness of these methods individually and in combination is assessed. The summary is given in Table 2.

Zhao et al. introduce bubble injection, wavy strip turbulator (WST), and nanofluid application in a double tube HX. Each technique is studied separately for heat enhancement. The bubble injection, WST, and nanofluid show enhancements in heat transfer of 66%, 74%, and 17%, respectively. Combining all three techniques results in a 144% increase in heat transfer. The optimum performance is shown by the combination of a bubble flow rate of 6 LPM, 150-degree angle WST (Figure 9), and 1% nanofluid concentration. It exhibits 2.49 times increase in heat transfer and a 10.33 times increase in pressure difference compared to a straight tube HX [49]. Luo et al. introduce a perforated wavy strip turbulator (PWST) (Figure 10). The findings indicate that the nanofluid, the PWST, and the bubble injection increase heat transfer by 56%, 53%, and 14.1% respectively. Moreover, combining all three techniques improves heat transfer and exergy losses by up to 2.15 and 1.82 times, respectively compared to a standard pipe. The optimal configuration, which involved a PWST with a hole diameter ratio of 6 and bubble injection with a flow rate of 6 LPM, yields a maximum PEC of 1.24 [50]. Wang et al. employ a helical coiled wire (HCW) turbulator along with bubble injection in double pipe HX. By varying the bubble injection flow rate between 2 and 5 LPM and adjusting the HCW pitch from 2.5 to 10 mm, they evaluate the PEC. The bubble injection, the HCW turbulator, and combining both methods result in heat transfer improvements of 66%, 78%, and 156%, respectively. The combined use of both methods provides superior thermal performance compared to their standalone applications, with a maximum PEC of 1.28 [51].

Al-darraji et al. enhance the heat transfer performance of the vertical shell and tube HX by introducing baffles of different designs and by injecting air bubbles into the shell

**Table 2.** Heat enhancement using air bubble injection

| Author | Year | HX type | Turbulator | Working Fluid | Air bubble flow rate | Analysis type | Key findings |
|---|---|---|---|---|---|---|---|
| Zhao et al. [49] | 2022 | Double pipe HXs | WST | CuO-water (1% concentration) | 6 LPM | Experimental | Increases heat transfer by 144%. |
| Luo et al. [50] | 2024 | Double pipe HXs | PWST | CuO-water (0.25% to 1% vol. fraction) | 2 to 6 LPM | Experimental | The highest PEC of 1.24 is achieved with a hole diameter ratio of 6 and 6 LPM air flow rate. |
| Wang et al. [51] | 2023 | Double pipe HXs | HCW | Water | 2 to 5 LPM | Experimental | Increases heat transfer by 156%. The PEC peaks at 1.28. |
| Al-darraji et al. [52] | 2024 | Shell and tube HX | Single segmental baffle, disc and ring baffle, and disc and ring with circular holes | Water | $10x10^{-5}$ $m^3/s$ | Experimental | The disc and ring with circular holes exhibit the highest effectiveness, ranging from 202% to 231%. The maximum PEC of 4.5 is achieved at a mass flow rate of 0.23 kg/s. |
| Zhou et al. [53] | 2022 | HSHTE | -- | Water | 1 to 5 LPM | Experimental | An increase in air bubble volume fraction increases the thermal performance of the HX. |

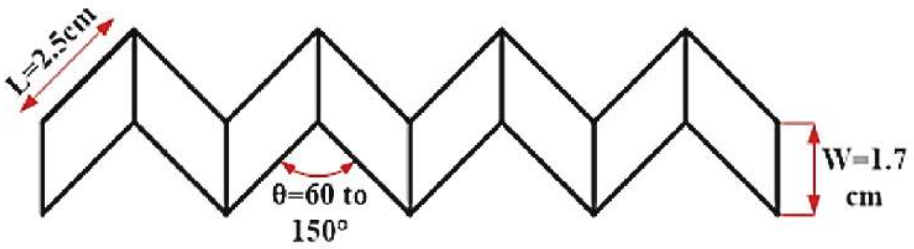


**Figure 9.** Wavy strip turbulator. [From Zhao et al. [49], with permission from Elsevier.]

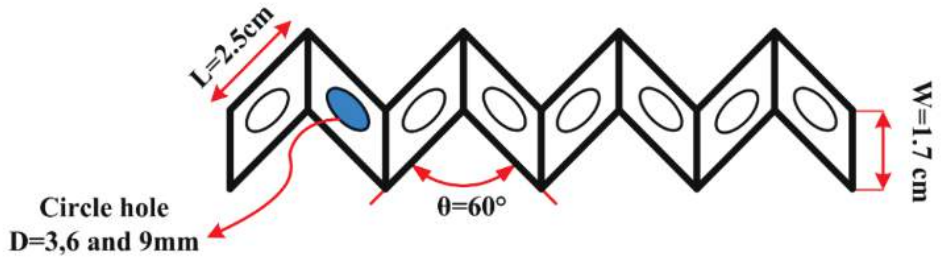


**Figure 10.** Perforated wavy strip turbulator. [From Luo et al. [50], with permission from Elsevier.]

side of the fluid. Experiments are conducted with varying cold-water flow rates and different baffle configurations. Figure 11 illustrates three configurations of baffles for shell and tube HX: (a) Single segmental baffle, (b) Disc and ring baffles, and (c) Disc and ring baffles having circular holes. The results show that the effectiveness improves with an increase in cold-water mass flow rates. With an air injection flow rate of $10^{-5}$ $m^3/s$, an improvement of 202% to 231% in effectiveness is observed for the configuration (c). The maximum PEC of 4.5 is achieved at a mass flow rate of 0.23 kg/s [52]. Zhou et al. introduce air bubbles from a 3 mm diameter tube into the horizontal shell and helically coiled

(a) (b) (c)

**Figure 11.** Three baffle configurations for shell and tube HX (a) single segmental baffle, (b) disc and ring baffle, and (c) disc and ring with circular holes baffle. [From Al-darraji et al. [52], with permission from Elsevier.]

tube exchanger (HSHTE). The increase in volume fraction results in a 4.5-fold increase in the number of thermal units, a 2.4-fold increase in first-law efficiency, and a 12.5-fold increase in exergy destruction [53].

**Heat Enhancement Using Vortex Generators**

In this section heat enhancement techniques based on the use of extended surfaces positioned in the path of flow are reviewed. These additional surfaces or vortex generators (VG) disturb the uniform flow of the fluid, reducing boundary layer thickness and increasing heat transfer. The method involves strategically positioning the VGs to maximize turbulence and improve heat transfer efficiency. There are different types of VGs depending upon their size and shape, as mentioned in Table 3.

Rastan et al. examine the use of longitudinal VGs in mini-channel HXs. The experimental and numerical studies exhibit a three-times improvement in the convection heat transfer as compared to without VRs [54]. Aridi et al. study the trapezoidal VR in a concentric tube HX. Through

**Table 3.** Heat enhancement using vortex generator.

| Author | Year | HX type | Vortex Generator | Analysis type | Key findings |
|---|---|---|---|---|---|
| Rastan et al. [54] | 2020 | Mini channel HXs | Longitudinal | Experimental and computational | Improves convective heat transfer by up to threefold. |
| Aridi et al. [55] | 2022 | Concentric tube HX | Trapezoidal | Computational | Improves heat transfer ratio by 97% and achieves a 2.1 PEC. |
| Hassan et al. [56] | 2022 | Double-tube HX | Cut square tape | Experimental | The 2.5 mm wide square-cut turbulator demonstrates a 271.7% increase in Nu value, while the hot water temperature difference rises by 113.7%. |
| Vahidifar et al. [57] | 2023 | HX tube design | Ring, disk, and O-ring inserts | Computational | The ring inserts show the highest increase in the Nu, achieving 2.92 times that of the smooth pipe. |
| Salhi et al. [58] | 2022 | Concentric double tube HX | Optimizing circular baffle pitches | Computational | Decreasing the inter-turbulator distance increases both the Nu and friction factor. Among different pitches, the 48 mm pitch demonstrates the highest PEC of 2.71. |
| Zhu et al. [59] | 2023 | HX tube design | TCR | Computational | Nu and friction increase by 52.3% to 65.8% and 92.7% to 202.3% across the range of Re. The maximum PEC of 1.335 is achieved at a pitch ratio of 0.5. |
| | | | TVR | | Nu and friction factor increase by 43.3% to 57.9% and 78.7% to 263.9% across the range of Re. |
| Zhao et al. [60] | 2023 | Fin-tube HX | Curved RWVG | Computational | Smaller offsets exhibit superior comprehensive performance. |
| | | | Straight RWVG | | Larger attack angles lead to increased heat transfer intensity and greater flow drag force. |
| Dadvand et al. [61] | 2019 | Microchannel | Rigid and flexible VG | Experimental and computational | The flexible VG enhances Nu, mixing index, and PEC by 18.46%,16.86%, and 42%, respectively, and reduces the friction factor by 42.33%, compared to rigid VG. |
| Mousavi et al. [62] | 2022 | double-pipe HX | Airfoils with zero angles of attack | Experimental | The maximum PEC of 1.91 is achieved at a Re of 6000, a thickness of 0.3, and a pitch ratio of 1.11. |

numerical simulation, they explore multiple positions of the VG in the annulus and tube region. The best performance is observed when VGs are inserted into the inner wall of the tube (Figure 12). This configuration leads to a 97% enhancement of the heat transfer ratio at a Re of 8000 for the cold fluid and 2000 for the hot water. A PEC of 2.10 is achieved under these conditions [55]. Hassan et al. test new copper VGs in double-tube HXs. The experimental results show that reducing the width of the turbulator strip fins improves heat transfer characteristics in turbulent flow regimes. The 2.5 mm wide square-cut turbulator (Figure 13), shows a 271.7% increase in the Nu, and a 113.7% increase in hot water temperature difference compared to the smooth tube [56].

Vahidifar et al. perform a numerical simulation on different shapes of turbulators in a pipe with an equal blocking area (Figure 14). The ring-shaped turbulator shows a significant impact on enhancing heat transfer characteristics inside the tube. The highest increase in the Nu with the ring, disk, and O-ring is 2.92, 1.8, and 2.19, respectively. The overall performance increases by 16.2% at a Re of 24,000 [57]. Salhi et al. introduce small baffle turbulators to enhance heat transfer from hot air to cold water (Figure 15). The numerical simulation shows that reducing the inter-turbulator distance increases the Nu and friction factor. The turbulators with pitches of 260 mm, 108.57 mm, 67.27 mm, and 48 mm yield PECs of 2.36, 2.42, 2.53, and 2.71, respectively [58].

Zhu et al. introduce two bionic rib designs: triangular concave rib (TCR) and triangular convex rib (TVR) (Figure 16). The numerical simulation using the SST k-ω model shows that bionic ribs stimulate the development of a longitudinal and transverse swirl, thereby enhancing fluid mixing and temperature distribution. For a pitch ratio of 0.75 over the range of Re studied, it is found that the Nu increases by 52.3% to 65.8% for TCR and by 43.3% to 57.9% for TVR, while the friction factor increases by 92.7% to 202.3% for TCR and by 78.7% to 263.9% for TVR compared

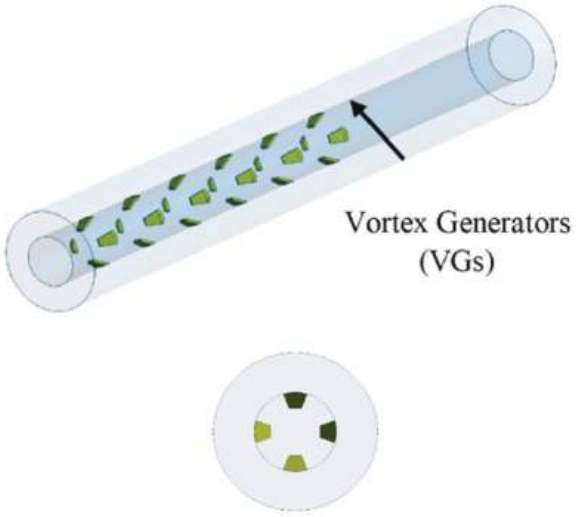


**Figure 12.** VG on the inner wall of the double-pipe HX tube. [From Aridi et al. [55], with permission from Elsevier.]

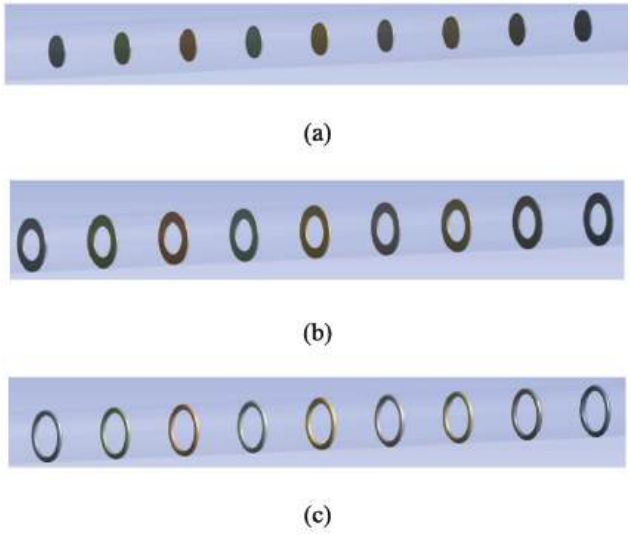


**Figure 14.** Various turbulator shapes inside the tube: (a) disk, (b) ring, and (c) O-ring. [From Vahidifar et al. [57], with permission from Elsevier.]

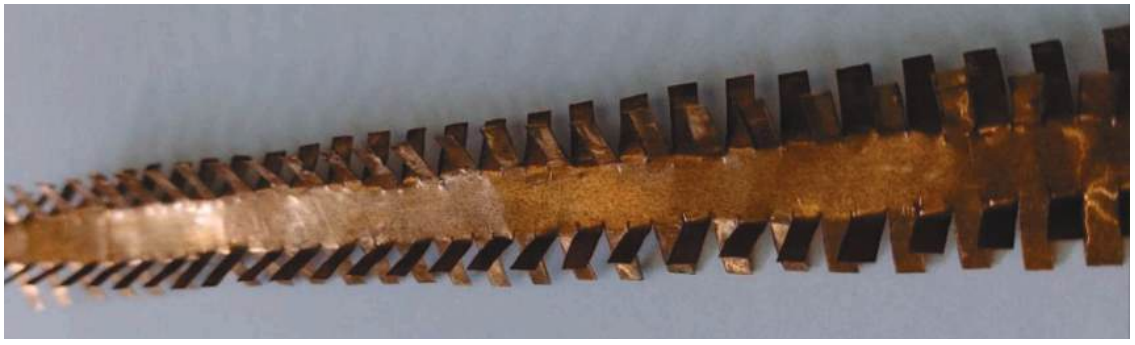

**Figure 13.** Square-cut copper VGs with a fin width of 2.5 mm. [From Hassan et al. [56], with permission from Elsevier.]

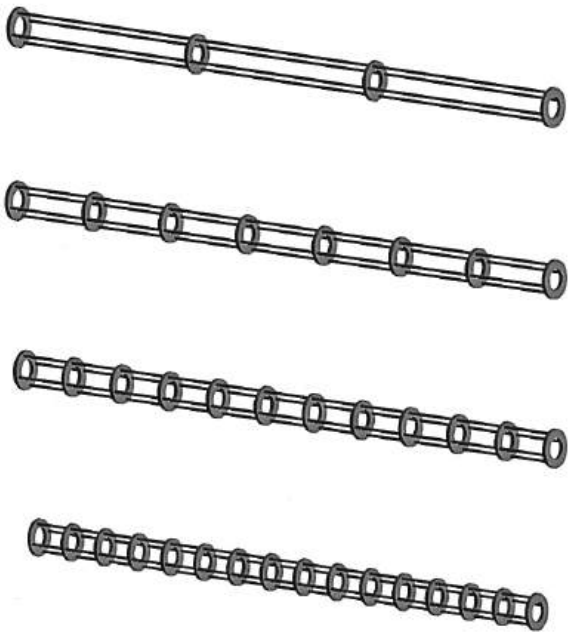

**Figure 15.** Circular baffle turbulators. [From Salhi et al. [58], with permission from Elsevier.]

to smooth tubes. The TCR achieves the maximum PEC of 1.335 at a pitch ratio of 0.5 [59]. Zhao et al. combine curved and straight rectangular winglet VG (RWVG) in the fin-tube HX. Through numerical simulation, the optimal location and size of RWVGs are selected. The curved RWVGs with a reduced offset exhibit superior overall performance, whereas the increased attack angle of the straight RWVGs leads to higher heat transfer intensity and increased drag force in the flow. The combination of the geometry parameters with z=0.5 mm, α= 100°, L= 2.0 mm, φ= 30, x=1.0 mm, and y= 5.5 mm (Figure 17) shows the highest PEC [60].

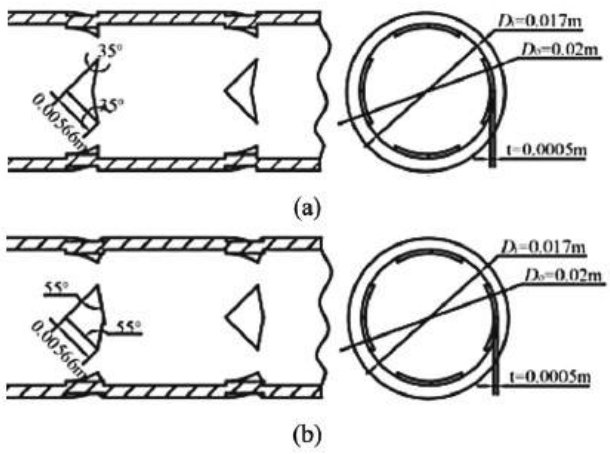


**Figure 16.** Longitudinal VGs with two bionic rib structures: (a) triangular concave rib and (b) triangular convex rib. [From Zhu et al. [59], with permission from Elsevier.]

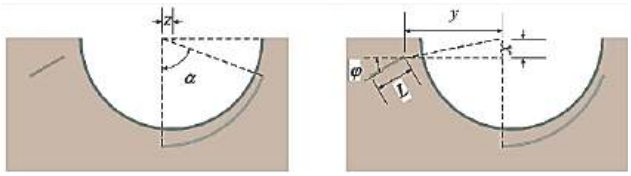


**Figure 17.** Straight and curved rectangular winglets VG. [From Zhao et al. [60], with permission from Elsevier.]

**Figure 18.** Airfoil-shaped turbulator with varying thickness profiles. [From Mousavi et al. [62], with permission from Elsevier.]

Dadvand et al. investigate a flexible beam as a VG on the lower wall of a microchannel. The beam oscillates by the motion of the fluid, producing secondary vortices from the tip of the beam. The numerical simulation shows that the Nu increases by 18.46%, the friction factor decreases by 42.33%, the PEC increases by 42%, and the mixing index increases by 16.86% compared to the rigid beam case [61]. Mousavi et al. perform experiments on four different shapes of airfoil turbulators with zero angles of attack for air as the working fluid (Figure 18). The Nu and friction factor increase with the pitch ratio and the thickness-to-length ratio of the airfoils. A maximum PEC of 1.91 is achieved at a Re 6000 with a 0.3 thickness-to-length ratio and 1.11 pitch ratio [62].

**Heat Enhancement Using Tape Inserts**

This section deals with the tape inserted in the HX to enhance the PEC with and without nanofluids as summarized in Table 4 and Table 5, respectively. Heat enhancement is achieved in the tubular HX using the additional structure placed in the pathway of flow, which results in the creation of vortices, reduction in boundary layer thickness, and enhancement of heat transfer. The working strategy involves implementing and evaluating different tape inserts to determine their effects on heat transfer performance and to analyze how changes in thermophysical properties affect this performance, both with and without the addition of nanofluids.

Vishwakarma et al. perform experimentation to study flow regimes and heat transfer rates in a circular tube fitted with wavy-tape inserts (Figure 19). For a wavy tape with a 0.75 wave ratio and 0.8 width ratios, the transition begins at Re 2193, 2021, and 2029, and ends at 4016, 3997, and 3989

for heat fluxes of 1, 2, and 3 kW/m$^2$, respectively. At a heat flux of 3 kW/m$^2$, the laminar flow region showed a maximum PEC of 1.9 with a wavy tape insert [63]. Farnam et al. investigate twisted tape inserts in straight and twisted tubes as shown in Figure 20. The experiments demonstrate that the heat transfer and pressure drop increase with a decrease in the twist ratio of twisted tape. The twisted tape, when used in combination with the twisted tube, exhibits higher Nu and friction factors compared to the straight tube. The twisted tube with an insert shows the maximum PEC of 2.28, at the lowest Re and twist ratio [64]. Luo et al. assess the impact of using the Special Shape Twisted Tape Turbulator (SSTT) and the HCW turbulator separately and together as shown in Figure 21. The SSTT turbulator is examined with opening distances between 0 and 4 mm, while the HCW turbulator is tested with pitch values between 5 and 20 mm. The study shows that the SSTT turbulator enhances heat transfer by 2.07 times and pressure drop by 7.4 times

**Table 4.** Heat enhancement using tape inserts.

| Author | Year | HX type | Tape insert | Analysis type | Key findings |
|---|---|---|---|---|---|
| Vishwakarma et al. [63] | 2024 | Circular tube HX | Wavy | Experimental | The laminar flow regime shows a maximum PEC of 1.9 at a heat flux of 3 kW/m$^2$. |
| Farnam et al. [64] | 2018 | Straight and twisted tube HX | Twisted | Experimental | Twisted tubes with inserts show higher Nu and friction factors. The maximum PEC of 2.28 is attained using a lower twist ratio tape in the tube at a minimal Re. |
| Luo et al. [65] | 2024 | Circular tube HX | SSTT and HCW | Computational | SSTT shows a maximum PEC of 1.22 with a 2 mm gap distance. The SSTT and HCW combination shows a maximum PEC of 1.31. |
| Forooghi et al. [66] | 2017 | Flat-tube HXs | Non-symmetrical bumps | Computational | Enhances heat transfer but is unfavorable during laminar-turbulent regime transitions. |
| Heeraman et al. [67] | 2023 | Double pipe HX | Dimple on twisted tape | Experimental | The Nu peaks at a D/H ratio of 3, reaching 111 at Re 13987. |
| Farhadi et al. [68] | 2024 | Coiled HX | Perforated and imperforated twisted tape | Computational | Imperforated twisted tape yields a maximum PEC of 1.55 in laminar flow at Re 2000. |
| Ifraj et al. [69] | 2023 | Tubular HX | Y-shape inserts with hexagonal, trapezoidal, kite, and hybrid shapes geometries and PI | Computational | The trapezoidal configuration with a PI of 20% achieves the highest PEC of 3.68 with air as the working fluid. |

**Table 5.** Heat enhancement using tape insert with nanofluid

| Author | Year | Tape insert | Nanofluid | Analysis type | Key findings |
|---|---|---|---|---|---|
| Gnanavel et al. [70] | 2020 | Twisted tape with rectangular cuts | $TiO_2$, BeO, ZnO and CuO | Computational | $TiO_2$ nanofluid with inserts shows a maximum PEC of 1.55 in the laminar region. |
| Azhari et al. [71] | 2023 | Twisted tape | CuO/water | Computational | At a Re of 20000, the maximum Nu is 285.8. |
| Saini et al. [72] | 2023 | Twisted tape | Carbon nanotubes/$H_2O$, $Al_2O_3/H_2O$, and $SiO_2/H_2O$ | Computational | Carbon nanotubes/$H_2O$ exhibit the maximum Nu of 143, followed by $SiO_2/H_2O$ at 140.12, and $Al_2O_3/H_2O$ at 136.68. A 3% volume concentration of nanofluid is used. |
| Kumar et al. [73] | 2022 | TTI, PTTI, DTTI | THNF | Computational | The combinations of DTTI with THNF ($Al_2O_3$ + Graphene + MWCNT) are the most effective. |
| Das et al. [74] | 2023 | TTT and RRTT | Therminol55(TH55)/MXene + $Al_2O_3$ | Computational | The maximum increase in the Nu is 11.04% when 0.2 wt.% nanofluid is used instead of water, and up to 105% with the addition of RRTT compared to a plain tube. |

compared to a smooth tube. The maximum PEC of 1.22 is achieved by the SSTT turbulator with a 2 mm opening distance. Combining both turbulators increases heat transfer and pressure drop by 2.42 times and 9.6 times, respectively, thereby representing a PEC of 1.31 [65].

Forooghi et al. explore the impact of non-symmetrically distributed bumps on the inserts, as shown in Figure 22. The numerical simulation finds that the non-symmetric insert distribution is unfavorable during laminar-turbulent regime transitions. Moreover, the study shows that the flow is fully laminar at 1000 Re, transitions at 1500 Re, and becomes turbulent at 2710 Re. The presence of a bypass region diminishes the potential for heat transfer enhancement [66]. Heeraman et al. investigate the impact of dimples on twisted tape inserts, as shown in Figure 23. The study examines dimples and protrusions with varying diameters and diameter-to-depth (D/H) ratios over a tube length of 1500 mm. The results show that the Nu reaches its peak at a D/H ratio of 3, with a value of 111 at a Re of 13987. The lowest value of friction factor is achieved at a D/H of 4.5, measured at 0.1033 at a Re of 13987. The maximum PEC of 1.088 occurs at a dimple diameter of 4 mm with a D/H of 4.5 at a Re of 6180 [67]. Farhadi et al. investigate the perforated and imperforated twisted tape insert (Figure 24). The best performance is attained in the laminar regime at a Re of 2000 using an imperforated twisted tape with a twist ratio of 15.73. The highest PEC in the laminar regime is 1.55, and in the turbulent regime, it is 0.99 [68]. Ifraj et al. examine Y-shape inserts with hexagonal, trapezoidal, and kite designs, as well as a combination of all three shapes, using perforation indexes (PI) of 10%, 20%, and 30% (Figure 25). The numerical simulations are performed using air, with Re varying from 3000 to 21000. The trapezoidal designs show a maximum Nu of 225 and a minimum friction factor of 0.07 with a PI of 20% at Re of 21000. Moreover, the trapezoidal insert achieves the highest PEC of 3.68 [69].

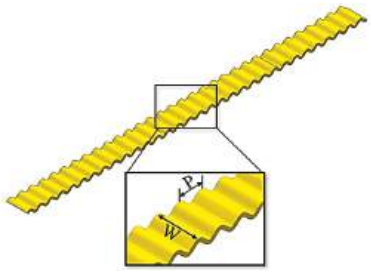


**Figure 19.** Wavy tape insert for circular pipe. [From Vishwakarma et al. [63], with permission from Elsevier.]

Some of the researchers study the tape inserts along with nanofluid to enhance the heat transfer. Gnanavel et al. modify the existing geometry of the twisted tape insert by adding the rectangular cuts (Figure 26). The thermal conductivity of the fluid medium is increased using nanofluids. The results show that the heat transfer increases with the increase in flow velocity. The $TiO_2$ nanofluid is found to be the most effective option for the HX in combination with a twisted tape

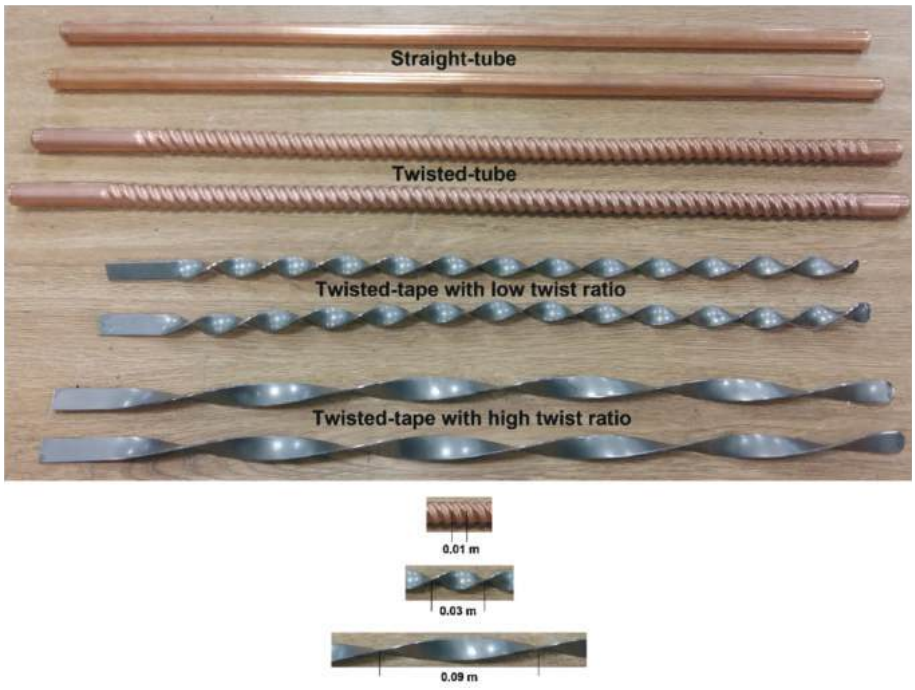


**Figure 20.** Straight and twisted tubes with twisted tapes of lower and higher twist ratios. [From Farnam et al. [64], with permission from Elsevier.]

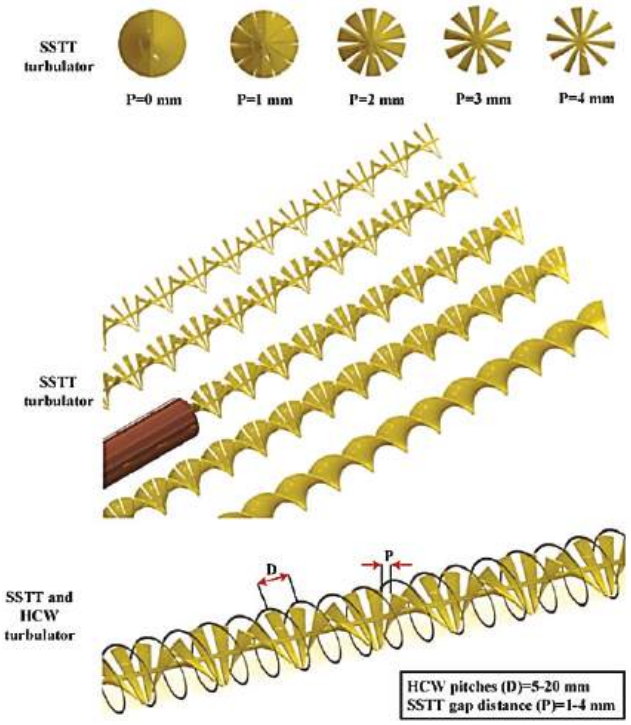


**Figure 21.** Geometric configuration of the special shape twisted tape turbulator (SSTT) and the helical coiled wire (HCW) turbulator. [From Luo et al. [65], with permission from Elsevier.]

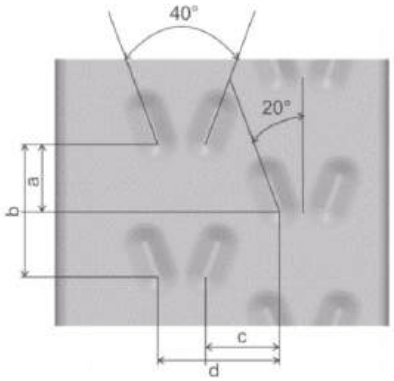


**Figure 22.** Non-symmetric distribution of inserts. [From Forooghi et al. [66], with permission from Elsevier.]

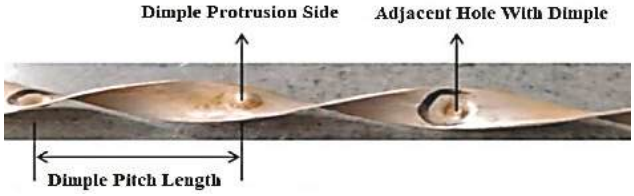


**Figure 23.** Twisted tape insert with variable hole diameter and depth for dimples. [From Heeraman et al. [67], with permission from Elsevier.]


**Figure 24.** (a) Imperforated and (b) perforated twisted tape insert. [From Farhadi et al. [68], with permission from Elsevier.]

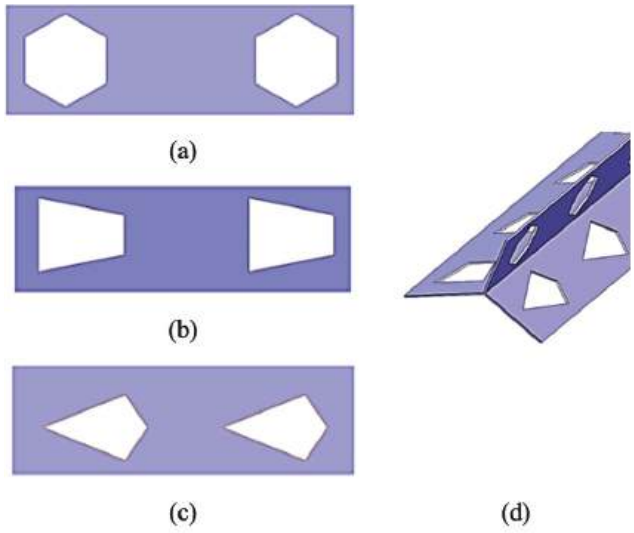


**Figure 25.** The geometric configuration of various metallic inserts: (a) hexagonal, (b) trapezoidal, (c) kite, and (d) hybrid. [From Ifraj et al. [69], with permission from Elsevier.]

insert yielding a maximum PEC of 1.55 in laminar flow [70]. Azhari et al. numerically evaluate twisted tape inserts, using the CuO/water-based nanofluid. The study finds that Nu and frictional entropy generation increase, whereas friction factor and thermal irreversibility decrease with an increase in Re. At a Re of 20000, the maximum Nu is 285.8 for the twisted tape insert and 156.1 for the plain tube. The results indicate that nanofluids and twisted tapes decrease the exergy losses and enhance heat transfer performance in HXs [71]. Saini et al. explore the use of twisted tape inserts with nanofluid. The results show a 6.03%, 16.74%, and 6.74% increase in the overall heat transfer coefficient with a 3% volume concentration of carbon nanotubes, $Al_2O_3$, and $SiO_2$ nanofluids in water, respectively. The maximum Nu is found to be 143 for carbon nanotubes, 136.68 for $Al_2O_3$, and 140.12 for $SiO_2$ [72].

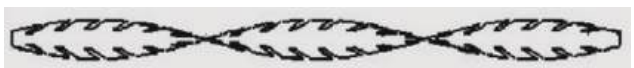

**Figure 26.** Twisted tape with rectangular insert. [From Gnanavel et al. [70], with permission from Elsevier.]

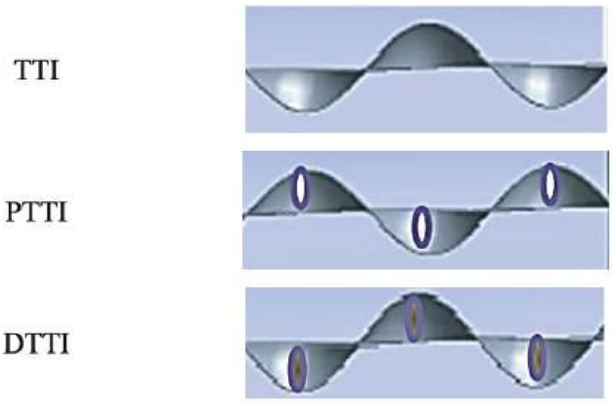


**Figure 27.** Geometric configuration of twisted turbulator insert (TTI), perforated twisted turbulator insert (PTTI), and dimpled twisted turbulator insert (DTTI). [From Kumar et al. [73], with permission from Elsevier.]

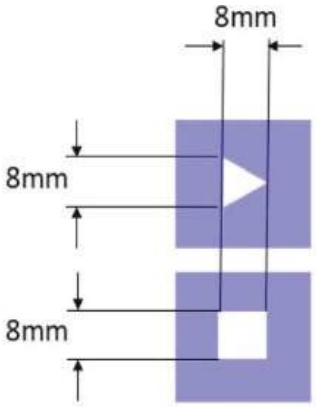


**Figure 28.** Triangular and rectangular ribbed twisted tape (TRTT& RRTT) inserts. [From Das et al. [74], with permission from Elsevier.]

Kumar et al. study the compact air HXs using water-based tripartite hybrid nanofluids (THNFs) with multiple inserts like twisted turbulator insert (TTI), perforated twisted turbulator insert (PTTI), dimpled twisted turbulator insert (DTTI) as shown in Figure 27. The study shows that the nanofluids alone do not significantly enhance the performance of HX, but the combination of THNFs ($Al_2O_3$ + Graphene + MWCNT) with turbulator inserts improves thermohydraulic performance at a lower Re. The DTTI with THNF is the most efficient for heat transfer enhancement, while the $Al_2O_3$ + CuO + Graphene combination of THNF should be avoided due to higher pressure drop [73]. Das et al. numerically examine the triangular and rectangular ribbed twisted tape (TTT and RRTT) inserts (Figure 28) with Therminol55(TH55)/MXene + $Al_2O_3$ nanofluid. An increase of 11.04% in the Nu is observed using the nanofluid as compared to water. The combination of nanofluid with RRTT increases the Nu up to 105% compared to a plain tube. The highest PEC of 1.67 is achieved with the combination of TH55 + $Al_2O_3$ and RRTT insert [74].

**Heat Enhancement Through Surface Modifications**

Heat enhancement is achieved by creating microstructures or fins on the heated surface, which induce turbulence in the fluid flow and reduce the thermal boundary layer as mentioned in Table 6. This approach focuses on designing and testing these microstructures or fins through experimental and numerical methods to enhance PEC.

There are different methods of creating microstructure on the surface, Nguyen et al. use electrochemical etching to create micro-surfaces on the plate of the HX. This method produces a uniform structure with an accurate thickness. The results show that at a roughness of 1.1 μm, there is a 10% to 18% enhancement in the overall heat transfer coefficient, a 28% to 53% increase in the friction factor, and a 1.05 to 1.21 increase in the PEC compared to a smooth surface [75]. Khalaf-Allah et al. use wire-cutting machines, laser processing, and sandpaper to create microstructures on copper surfaces (Figure 29). The heat transfer coefficients are measured using distilled water at varying heat fluxes. The results show that microstructured surfaces outperform smooth surfaces, with 31.3% to 78.5% improvements in heat transfer over the range of Re. The combination of the above-mentioned techniques provides better performance than a single technique, with enhancements of 51% to 92% at different conditions [76].

Moharana et al. use the deformational cutting method to make a semi-closed microstructure on a tube bundle surface (Figure 30). The microstructure increases the wall surface area which initiates wall boiling earlier as compared to the smooth surface. The tube bundle with microstructure has shown higher effectiveness and outperforms the smooth tube bundle by more than 100% [77]. Alnaimat et al. embed square in-line pin-fins in the flat plate as shown in Figure 31. The HX with pin-fins exhibits the same effectiveness as that of a flat plate at low Re. As the Re increases, HXs with pin-fins become more effective. The maximum enhancement in effectiveness reaches 84% for Cr (the ratio of the fluid's minimum to maximum heat capacity) of 1 and 66% for Cr of 0.5 across different flow conditions compared to flat pate [78]. Dizjeh et al. create three different textured surfaces on the tube having features like inward-facing elements, a wire coil, and spiral corrugations (Figure 32). The numerical simulation is performed at 90,000 Re and 0.836 Prandtl number (Pr). The findings indicate that the inward-facing ellipsoidal elements exhibit the highest performance, achieving a 22% to 42% increase in heat transfer and a 41% to 97% increase in pressure drop across the range of Re [79].

Alteneiji et al. introduce gyroid and primitive designs for compact cross-flow HX using complex macrostructures

**Table 6.** Heat enhancement using micro-surfaces

| Author | Year | Generation technique or micro-surface type | Working fluid | Analysis type | Key findings |
|---|---|---|---|---|---|
| Nguyen et al. [75] | 2024 | Electrochemical etching | Water | Computational | The roughness of 1.1 μm improves the overall heat transfer coefficient by 10% to 18%, with a 28% to 53% growth in the friction factor compared to a smooth surface, while PEC values range from 1.05 to 1.21. |
| Khalaf-Allah et al. [76] | 2023 | Wire-cutting machines, laser processing, and sandpaper | Water | Experimental | The combined technique outperforms single techniques, with enhancements of 51% to 92% in pool boiling. |
| Moharana et al. [77] | 2023 | Deformational cutting | Water | Experimental | Microstructure on tube bundles outperforms smooth tube bundles by over 100%. |
| Alnaimat et al. [78] | 2021 | Square in-line pin-fins | Water | Computational | More effective as the Re increases but consumes more power, with a maximum increase in effectiveness of 84% for Cr = 1 and 66% for Cr = 0.5. |
| Dizjeh et al. [79] | 2022 | Inward-facing elements, a wire coil, and spiral corrugations | Water | Computational | Inward-facing ellipsoidal elements show the highest performance with a 22 to 42% increase in heat transfer alongside a 41 to 97% rise in pressure drop across the range of Re. |
| Alteneiji et al. [80] | 2022 | Gyroid and primitive structure | Water | Computational | The gyroid structure improves the HX effectiveness by 35% with a maximum pressure drop of 4 Pa compared to the primitive structure. |
| Yan et al. [81] | 2024 | Gyroid structure | Water | Experimental and computational | The gyroid structure shows better PEC compared to offset strip fin, 15° zigzag channel PCHE, circular tube, and chevron-type plate HX and is comparable to offset strip fin HX. |
| Liu et al. [82] | 2023 | Reversed trapezoidal profile fins | Air | Computational | At 14500 Re, increasing the fin angle from 2° to 10° results in a 13% increase in Nu and a 51% increase in pressure drop. |
| Soheibi et al. [83] | 2022 | Slotted fins | Air | Computational | The presence of three slots on the fins reduces the drag coefficient by 23% and increases the Nu by 76%. Oscillation of tubes and slotted fins further improves heat transfer up to 2.5 times. |
| Searle et al. [84] | 2024 | Helical pin fin tube | $sCO_2$ | Experimental and computational | A 14% improvement in the Nu is observed at an equal friction factor and a 4-time reduction in the friction factor is noticed at equal Nu. |
| Tariq et al. [85] | 2023 | Fins inside the pipe | Graphene oxide 0.1% concentration | Computational | Adding nanoparticles enhances the effectiveness by a maximum of 7%. Reducing the speed of hot fluid from 6 m/s to 2 m/s increases effectiveness by approximately 33.3%. |

known as triply periodic minimal surfaces (TPMS) (Figure 33). Numerical simulation shows that the complex topology of the gyroid structure increases the effectiveness of the compact HX by 35% compared to the primitive structure and exhibits a maximum pressure drop of 4 Pa [80]. Yan et al. use a 3D printer to develop a Gyroid-structured from stainless steel using a laser melting technique (Figure 34). Experimental and numerical evaluations are conducted using water as the working medium. The heat transfer performance of the Gyroid-structured HX exceeds that of the offset strip fin, 15° zigzag channel printed circuit heat exchanger (PCHE), circular tube, and chevron-type plate HX. The Gyroid-structured HX shows a higher pressure drop with an increase in Re, resulting in a PEC comparable to the offset strip fin HX and higher than the rest of the HX designs [81].

Liu et al. develop a reversed trapezoidal profile fins for staggered tube HX (Figure 35). The model is tested with different fin angles (2° to 10°), lengths (0.5D to 2D), and thicknesses (1 mm to 5 mm) over a range of Re (5500 to

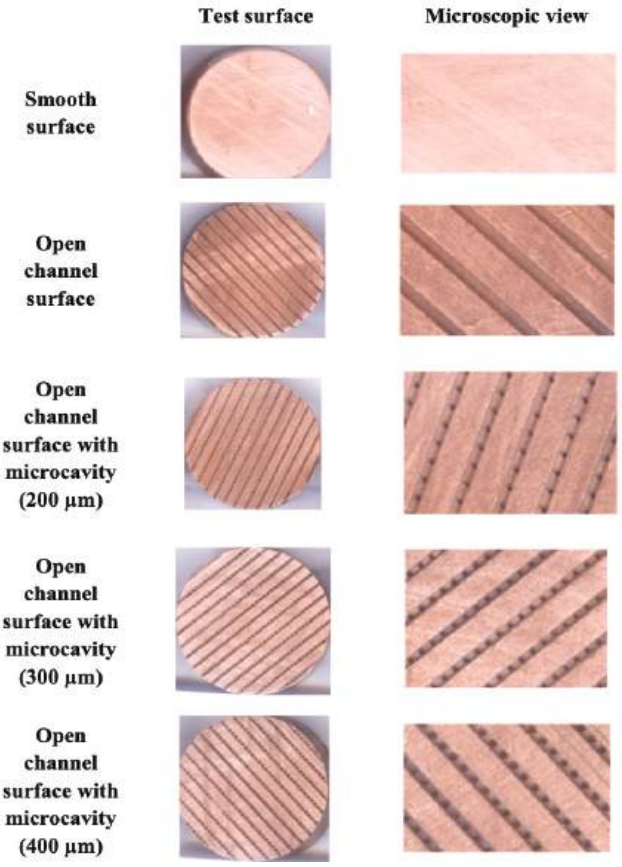


**Figure 29.** Different images of microstructured surfaces on copper plate. [From Khalaf-Allah et al. [76], with permission from Elsevier.]

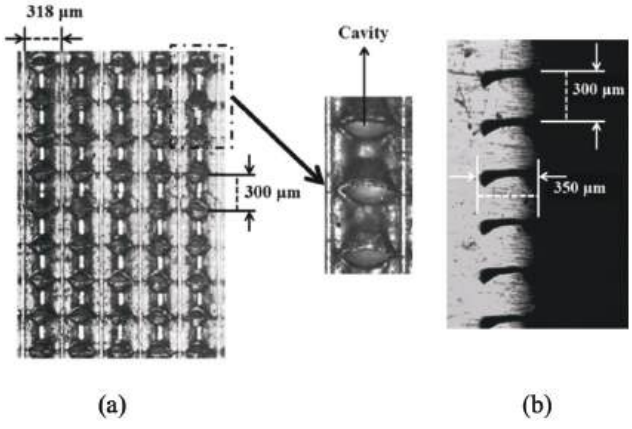


**Figure 30.** Semi-closed microstructure (a) top view and (b) side view. [From Moharana et al. [77], with permission from Elsevier.]

14500). The numerical simulation shows that the larger fin lengths achieve higher heat transfer rates and lower flow resistance. In contrast, increasing fin thickness leads to a larger pressure drop than Nu improvement. For a

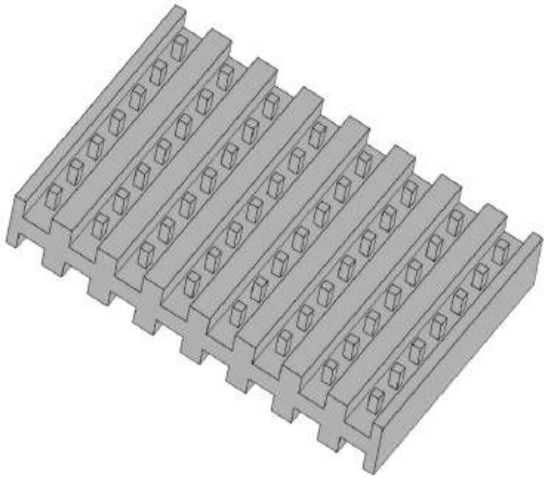

**Figure 31.** Microchannel square in-line pin-fins HX. [From Alnaimat et al. [78], with permission from Elsevier.]

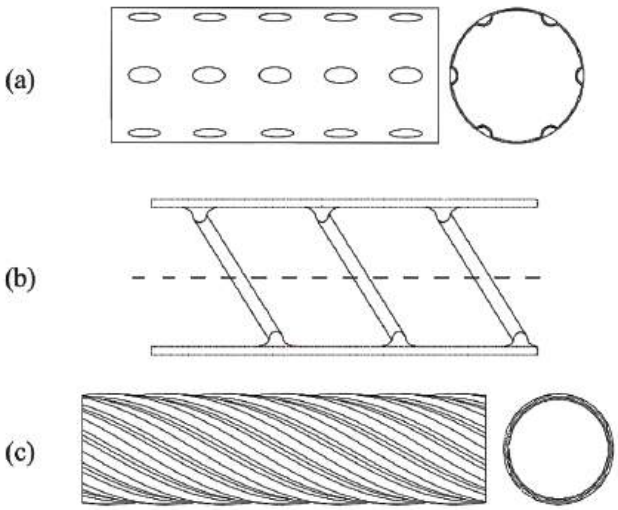


**Figure 32.** Different types of pattern structures: (a) ellipsoidal inward-facing elements, (b) a wire coil, and (c) spiral corrugations. [From Dizjeh et al. [79], with permission from Elsevier.]

Re of 14500, an increase in fin angle from 2° to 10° leads to a 13% increase in Nu and a 51% increase in pressure drop [82]. Soheibi et al. study the oscillation of tubes with slot fins on the tube to enhance heat transfer (Figure 36). Three slots on the fins reduce the drag coefficient by 23% and increase the Nu by 76%. The tube oscillation increases the heat transfer by 3% as compared to a fixed tube. Adding slotted fins to the oscillating tube bank increases heat transfer up to 2.5 times [83]. Searle et al. perform an experimental study of pin fin in a helical pattern inside a tube, as shown in Figure 37. The results show a four-time reduction in the friction factor at the equal Nu and a 14%

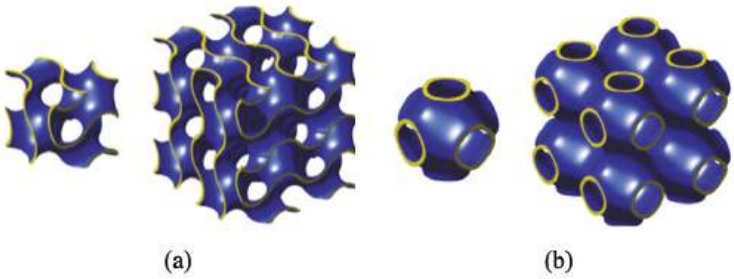


**Figure 33.** Triply periodic minimal surfaces (TPMS) structures-based compact HXs: (a) gyroid, and (b) primitive. [From Alteneiji et al. [80], with permission from KeAi.]

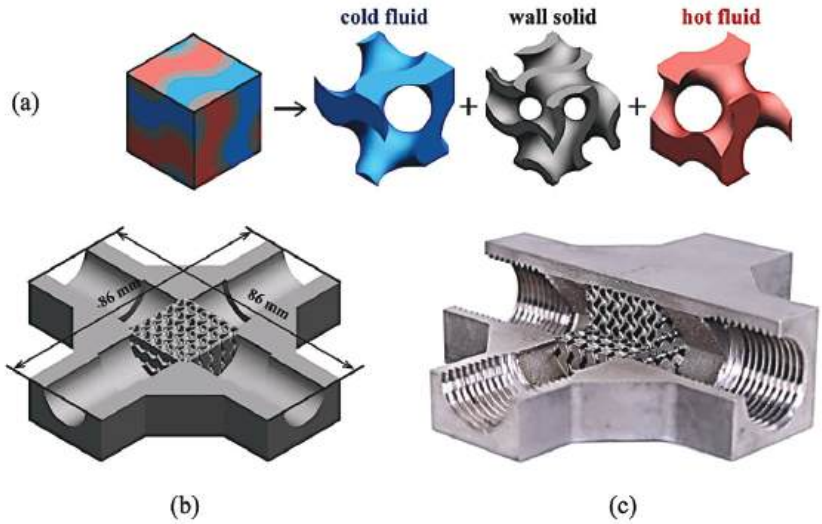


**Figure 34.** Geometric configuration of gyroid-structured HX: (a) computational domain, (b) complete numerical model, and (c) cut gyroid-structured. [From Yan et al. [81], with permission from Elsevier.]

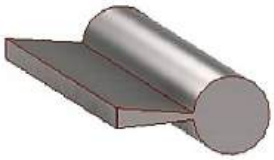

**Figure 35.** Reversed trapezoidal profile fins on the HX tube. [From Liu et al. [82], with permission from Elsevier.]

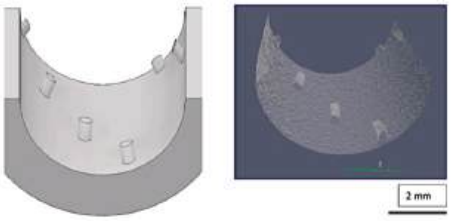


**Figure 37.** Helically coiled fin tube design. [From Searle et al. [84], with permission from Elsevier.]

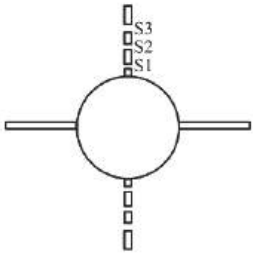


**Figure 36.** Geometric configuration of slots on the tube fin. [From Soheibi et al. [83], with permission from Elsevier.]

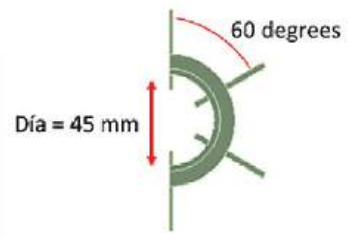


**Figure 38.** Finned tube HX (solid side). [From Tariq et al. [85], with permission from Elsevier.]

improvement in the Nu at an equal friction factor compared to the smooth tube [84]. Tariq et al. develop a new design for a finned HX (Figure 38) and use graphene oxide nanoparticles in the working fluid. The results show that reducing the speed of the hot fluid from 6 m/s to 2 m/s increases the effectiveness of the HX by 33.3%. Moreover, the study finds that the insertion of nanoparticles at a concentration of 0.1% enhances the effectiveness of the HX by a maximum of 7% [85].

**Heat Enhancement Using the Baffle**

Another method to enhance heat transfer involves introducing baffles into the fluid flow path as summarized in Table 7. The baffle plates produce a rotary flow pattern, enhancing the axial fluid flow and boosting the heat transfer rate [86]. In this approach, different shapes, angles, and positions of the baffles are analyzed to determine their effect on heat transfer enhancement.

Mazharmanesh et al. study heat enhancement on vertically heated surfaces using a flexible baffle. The moving baffle produces turbulence in the fluid with its to-and-fro motion, resulting in vortices in the natural convection path. The 2D numerical simulation shows that the heated wall with a flexible baffle enhances convection heat transfer by 12% compared to a rigid baffle. They also study the effect of attaching a baffle on the heated surface at different elevations from the bottom. The results show that changes in the normalized baffle elevation to 0.2, 0.3, and 0.5 across the range of Re result in 8% to 10%, 9% to 12%, and 7% to 8% enhancement in convection heat transfer, respectively [87]. Boonloi et al. study "X" and "V" shaped baffles in the laminar flow, as shown in Figure 39. Numerical simulations are performed to find the thermal-hydraulic performance of the two baffles. The V-shaped baffle shows the highest PEC of 4.07 [88].

Rahman et al. explore different angles of deflector baffle plates fitted in a smooth air duct (Figure 40). The experiment shows that increasing the angle of the baffles decreases the flow velocity and pressure drop. The results indicate that baffle angles of 30°, 40°, and 50° resulted in 70.8%, 66.3%, and 61.3% increases in fluid velocity compared to the smooth duct. The 30° baffle shows the highest PEC of 1.449, while the 40° and 50° baffles show PEC values of 1.148 and 1.141, respectively, compared to the smooth duct [89]. Abidi et al. use angled baffles to enhance heat transfer in a shell and tube HX. As the baffle angle increases, the Nu also increases. The maximum PEC of 1.55 is achieved with a baffle angle of 180° at a Re of 7500 [90].

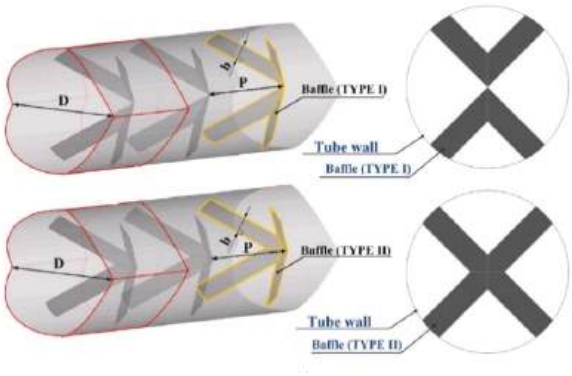


**Figure 39.** Geometric configuration of X-V baffles in the HX. [From Boonloi et al. [88], with permission from Elsevier.]

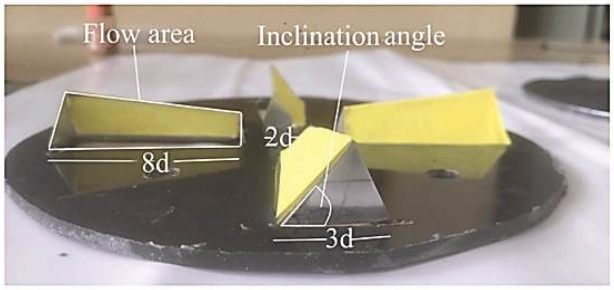


**Figure 40.** Pictorial view of the deflector baffle plate. [From Rahman et al. [89], with permission from Elsevier.]

**Table 7.** Heat enhancement using the baffles

| Author | Year | Geometry type | Working fluid | Analysis type | Key findings |
|---|---|---|---|---|---|
| Mazharmanesh et al. [87] | 2023 | Flexible baffle | -- | Computational | Replacing rigid baffles with flexible ones enhances heat transfer by up to 12%. |
| Boonloi et al. [88] | 2023 | X-V baffles | Air | Computational | V baffles show the highest PEC of 4.07. |
| Rahman et al. [89] | 2023 | Different angles of deflector baffle | Air | Experimental | 30° baffle shows the highest PEC of 1.449 compared to 40° and 50° baffle. |
| Abidi et al. [90] | 2023 | Effects of baffle angle | $Fe_3O_4$-MWCNT water hybrid nanofluid with a 4% volume fraction | Computational | The 180° baffle angle exhibits the maximum PEC of 1.55 at Re of 7500. |

**Printed Circuit Heat Exchanger**

PCHEs are designed to have a higher heat transfer rate area per unit volume compared to tube-type HXs. The higher power density of the PCHE results in the smaller size of the HX [91]. This approach focuses on optimizing the flow paths and adjusting geometric parameters to enhance heat transfer efficiency while minimizing the overall volume and pressure drop. There are different types of PCHE designs based on the geometry configuration, as described below:

**Straight Channel**

Table 8 shows the summary of the straight channel PCHE. In the straight channel PCHE, a straight flow path is configured with multiple possibilities for arranging the cold and hot plates in the assembly. Pandey et al. study the cooling of $sCO_2$ with water using various banking configurations as shown in Figure 41. They use a numerical tool to study the PCHE for a range of Re for the hot and cold fluids. The results reveal that the hot-cold-hot assembly of the plates provides the smallest possible volume (0.74 $m^3$) and the highest effectiveness of 99.7% compared to other banking configurations [92]. Zhong et al. introduce a novel PCHE with straight rectangular micro-channels for $sCO_2$ (Figure 42) and study the effect of primary and secondary fluid inlet temperatures on the system's heat transfer. Experiments are performed with a 10.3% rise in primary fluid inlet temperature. As a result, an increase of 89.0% is observed in the heat transfer rate. It is found that the effectiveness of the system is a function of the inlet temperature of the secondary fluid and increases by 23.3% with a 5.9% rise in the cold fluid inlet temperature [93]. Xu et al. investigate a double semicircular straight channel PCHE for Lead-Bismuth Eutectic (LBE) and $sCO_2$. The overall heat transfer coefficient is significantly enhanced with the change in the mass flux of the $sCO_2$ as compared to that

**Table 8.** Heat enhancement using straight channel PCHE

| Author | Year | Geometry type | Working fluid | Analysis type | Key findings |
|---|---|---|---|---|---|
| Pandey et al. [92] | 2024 | Straight channel | $sCO_2$ | Computational | The hot-cold-hot banking configuration provides the smallest possible volume (0.74 $m^3$) and the highest effectiveness of 99.7% compared to other banking configurations. |
| Zhong et al. [93] | 2023 | Rectangular straight channel | $sCO_2$ | Experimental | Heat transfer rate increases by 89.0% with a 10.3% rise in primary side inlet temperature, while effectiveness rises by 23.3% with a 5.9% increase in secondary side inlet temperature. |
| Xu et al. [94] | 2023 | D-type straight channel | LBE and $sCO_2$ | Computational | The smaller tube diameter and reduced wall thickness improve overall heat transfer efficiency in PCHE. |
| Li et al. [95] | 2024 | Straight channel | LBE and $sCO_2$ | Computational | Increasing the channel length is favorable for $CO_2$ and unfavorable for LBE due to higher pressure drop. At a maximum channel length of 900 mm, LBE and $sCO_2$ exhibit PEC values of 0.9 and 1.4, respectively. |
| Li et al. [96] | 2023 | Semicircular straight channel | Supercritical methane | Computational | Heat transfer peaks near the pseudo-critical point and decreases in film boiling. |
| Xu et al. [97] | 2023 | Straight channel | LBE and $sCO_2$ | Computational | PCHE shows a power density of 181 $MW/m^3$, which is eight times higher than that of shell-and-tube HX. |
| Lee et al. [98] | 2023 | Dotted straight channel | Water | Computational | A 66% improvement in the heat transfer rate is achieved without any increase in the pressure drop of the HX. |
| Tong et al. [99] | 2023 | NACA 0025 airfoil fin, rectangular fin, rhombic fin, and elliptical fin | Molten salt and $sCO_2$ | Computational | The rhombic fin demonstrates the highest heat transfer rate and the lowest synergy field. |
| Lao et al. [100] | 2019 | Discontinuous fin | Molten salt and $sCO_2$ | Computational | The Nu increases with the increase in velocity, while molten salt exhibits a higher pressure drop than $sCO_2$. |
| He et al. [101] | 2024 | Semi-circular and circular straight channels | Molten salt and $sCO_2$ | Computational | Achieves three times the heat transfer rate compared to a shell and tube steam generator. |

of LBE. Additionally, geometric parameters such as smaller tube diameter and reduced wall thickness also increase the system's heat transfer [94]. Li et al. analyze the heat transfer performance of a straight-channel PCHE for $sCO_2$ and LBE. An increase in the $sCO_2$ mass flow rate enhances the overall heat transfer performance, and higher pressure on the $sCO_2$ side improves thermo-hydraulic performance. Sensitivity to geometric parameters shows that increasing the channel width increases the heat transfer but also increases the HX volume. The channel length is favorable for $sCO_2$ but unfavorable for LBE due to the higher pressure drop. At a maximum channel length of 900 mm, LBE and $sCO_2$ exhibit PEC values of 0.9 and 1.4, respectively [95].

Li et al. investigate a 1.2 mm diameter semicircular channel for supercritical methane vaporization at the pseudo-critical point. Their numerical simulation reveals a peak in heat transfer at this point, followed by a decrease due to film boiling [96]. Xu et al. design a semicircular channel PCHE for a 280 $MW_{th}$ lead-bismuth HX for advanced nuclear reactors (Figure 43). The design demonstrates a power density of 181 $MW/m^3$, which is eight times greater as compared to shell and tube HX. Larger LBE inlet velocities or smaller channel diameters resulted in a reduced total volume and mass of the PCHE [97]. Lee et al. introduce a novel design for a PCHE using a mathematical model to optimize the layout of the channels. The model replaces the straight wall channel design with a dotted channel design, allowing cross-flow along the flow path (Figure 44). Numerical simulation shows a 66% improvement in heat transfer rate without any increase in the pressure drop of the HX [98].

Tong et al. study NACA 0025 airfoil fin, rectangular fin, rhombic fin, and elliptical fin design in the molten salt and $sCO_2$ PCHE (Figure 45). Numerical simulations reveal that the heat transfer rate increases with velocity. Among the designs, the rhombic fin exhibits the highest heat transfer rate, followed by the elliptical and NACA 0025 airfoil fins, which show similar values, with the rectangular fin showing the lowest. Additionally, the rhombic fin design displays the lowest synergy field. The molten salt achieves a maximum heat transfer rate of 210 kW, compared to 45 kW for $sCO_2$ at a velocity of 0.5 m/s with the rhombic fin [99]. Lao et al. introduce discontinuous fins into the flow path of molten salt and $sCO_2$ PCHE (Figure 46). Numerical simulations demonstrate that these discontinuous fins cause

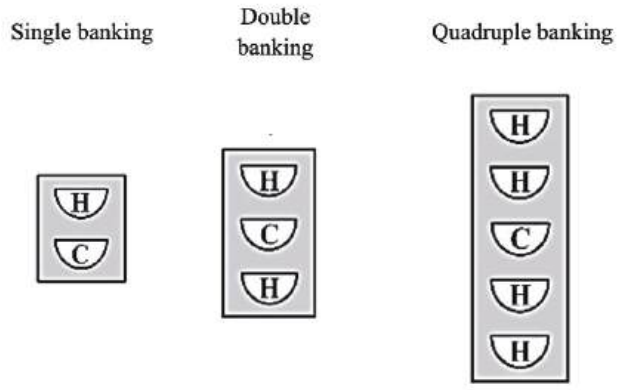


**Figure 41.** Different configurations of hot and cold plates in the PCHE. [From Pandey et al. [92], with permission from Elsevier.]

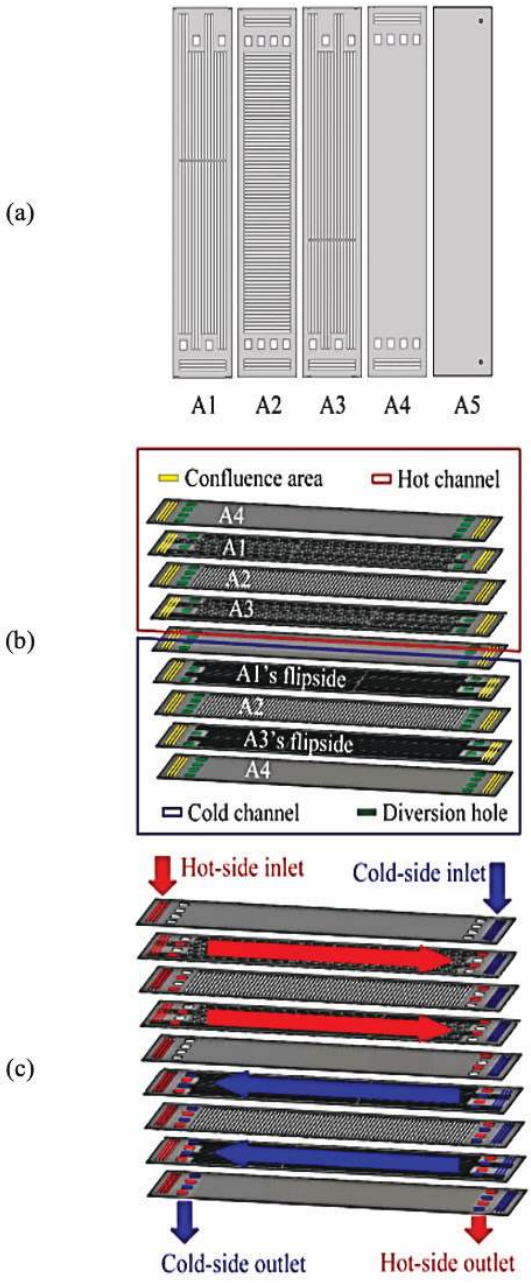


**Figure 42.** Novel PCHE with rectangular channels: (a) shape of the channels, (b) configuration of the different plates, and (c) flow path of the cold and hot fluid. [From Zhong et al. [93], with permission from Elsevier.]

flow separation and the generation of vortices within the fluid, leading to fluctuations in the heat transfer coefficient. Both the Nu and pressure drop increase with the velocity of the fluid; however, molten salt exhibits a greater pressure drop compared to $sCO_2$ [100]. He et al. explore printed circuit steam generators for high-temperature applications for molten salt thermal power systems (Figure 47). They improve the design by utilizing a combination of semi-circular and circular channels for a 50 $MW_{th}$ printed circuit steam generator. Numerical simulations show that this design achieves three times more heat transfer compared to a shell and tube steam generator [101].

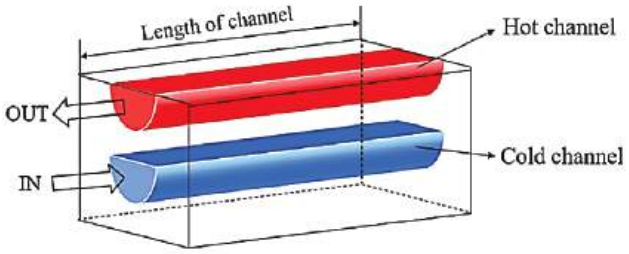


**Figure 43.** Semicircular PCHE design for a lead–bismuth fast reactor. [From Xu et al. [97], with permission from Elsevier.]

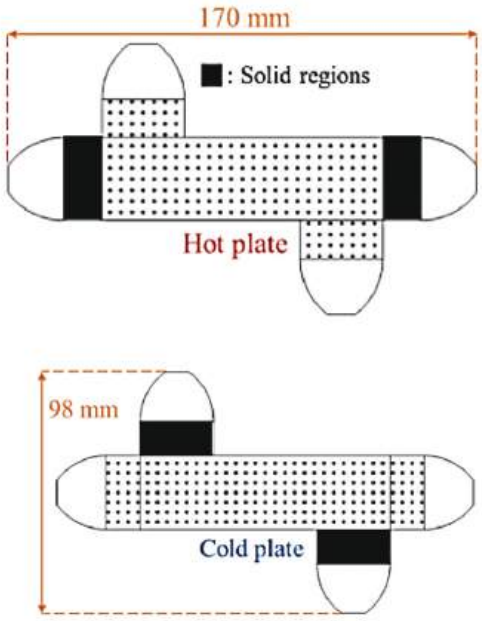


**Figure 44.** Geometric configuration of a novel PCHE design utilizing dual-fluid topology optimization. [From Lee et al. [98], with permission from Elsevier.]

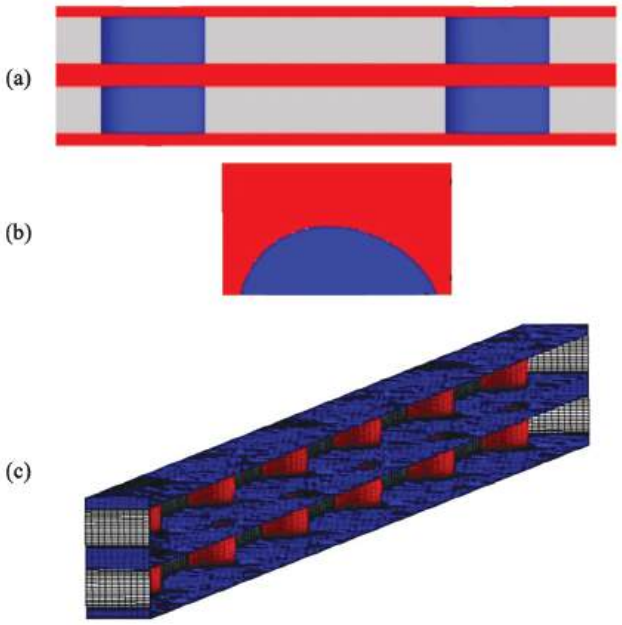


**Figure 46.** Discontinues fin in the PCHE: (a) side view, (b) fin top view, and (c) computational domain. [From Lao et al. [100], with permission from Elsevier.]

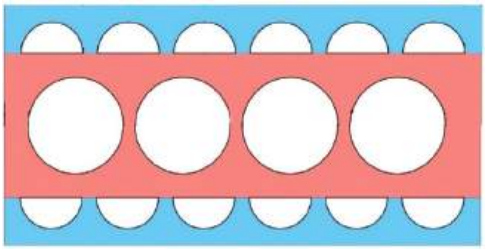

**Figure 47.** Cross-sectional view of the unit cell of the printed circuit steam generator for a molten salt reactor. [From He et al. [101], with permission from Elsevier.]

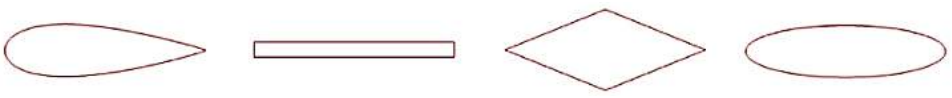


**Figure 45.** Geometric configuration of fin designs: (a) NACA 0025 airfoil fin, (b) rectangular fin, (c) rhombic fin, and (d) elliptical fin. [From Tong et al. [99], with permission from Elsevier.]

**Zigzag Channel**

Recently, researchers have designed the PCHE channels in a wavy or crisscrossed pattern to enhance the disturbance in the fluid flow path and consequently increase heat transfer, as summarized in Table 9. Liu et al. experimentally investigate zigzag channels for $sCO_2$ for Gen-IV nuclear reactors (Figure 48). Experimentation is performed on a 30° zigzag angle, 7.24 mm pitch, and 1.95 mm diameter of the channel for Re 3201 to 43258 and Pr 1.1 to 6.0. The zigzag channel presents a two-times enhancement in heat transfer and a seven-time increase in the friction factor compared to the straight channels [102]. Saeed et al. study the pumping load for different channel geometries in $sCO_2$-BC precoolers. They discover that straight channel precoolers cut pumping power in half compared to zigzag channels. Regardless of a slight decrease in cycle efficiency, the zigzag designs significantly reduce precooler size by three times [103]. Goto et al. investigate the straight and zigzag channel PCHE designs (Figure 49). Their findings show that the zigzag channel experiences an 11% improvement in the heat transfer coefficient and an 18% rise in pressure drop compared to the straight channel [104].

Ahmed et al. develop a zigzag channel PCHE for solar power applications using $sCO_2$ (hot fluid) and water (cold fluid) as working fluid. They study the effect of changing

**Table 9.** Heat enhancement using zigzag channel PCHE

| Author | Year | Geometry type | Working fluid | Analysis type | Key findings |
|---|---|---|---|---|---|
| Liu et al. [102] | 2023 | Zigzag channel | $sCO_2$ | Experimental | Enhances heat transfer by two times and friction factor by seven times compared to straight channels |
| Saeed et al. [103] | 2024 | Zigzag channel | $sCO_2$ | Computational | The HX size is reduced by three times, with a slight decrease in cycle efficiency due to the higher pressure drop. |
| Goto et al. [104] | 2023 | Zigzag channel | Refrigeration fluid (R1234ze(E) and R32) | Computational | There is an 11% increase in the heat transfer coefficient and an 18% rise in pressure drop compared to straight micro-channels. |
| Ahmed et al. [105] | 2023 | Zigzag channel | $sCO_2$ | Computational | Heat transfer improves by reducing water side inlet temperature and $sCO_2$ working pressure. |
| Liu et al. [106] | 2023 | Zigzag channel | $sCO_2$ | Computational | A novel cellular arrangement enhances overall heat transfer coefficients by 8.6% compared to traditional designs. |
| Khan et al. [107] | 2023 | Zigzag channel | Water | Computational | The PEC peaks at 1.45 with a bend angle of 35° and adding a straight section at the bend further enhances it to 1.5. |
| Wang et al. [108] | 2023 | Zigzag channel | $sCO_2$ | Computational | The addition of a straight section at each bend, decreases the friction factor by 33.1% to 84.7%, and Nu by 3.6% to 30.3%, resulting in improved PEC with a maximum enhancement of 45.9%. |
| Liu et al. [109] | 2024 | Combined straight and zigzag channel | LBE and $sCO_2$ | Computational | A 120° zigzag channel combined with a straight channel, exhibits a higher performance with a 12.6% increase in heat flux compared to straight channels on both sides. |
| Aakre et al. [110] | 2022 | Zigzag channel | Molten salt and $sCO_2$ | Experimental | The elliptical zigzag channel shows a friction factor of 3 to 5 times higher for molten salt and higher Nu compared to a straight circular channel. |
| Samarmad et al. [111] | 2023 | Zigzag channel | $sCO_2$ | Experimental and computational | Two-way corrugated with backward/forward-facing channels with an amplitude of 0.8 and angle of attack of 60° achieve a maximum Nu improvement of 78% and the highest PEC of 1.43. |
| Li et al. [112] | 2024 | Zigzag channel | $sCO_2$ | Computational | The maximum PEC of 1.21 is obtained with a $\lambda$ of 15.07 mm and an A of 1.73 mm. |
| Samarmad et al. [113] | 2023 | Zigzag channel | $sCO_2$ | Experimental and computational | A 78% increase in Nu is observed with an A of 0.8 and $\lambda$ of 12.6, but increases friction factor by 130%, with a PEC of 1.5 and a 27% boost in effectiveness. |

the hot and cold side inlet temperature and pressure on the performance of the HX. The results show that reducing the water inlet temperature and $sCO_2$ working pressure improves the performance of the HX [105]. Liu et al. introduce a new modification to the hot and cold fluid cellular arrangement in the zigzag channel, as shown in Figure 50. Numerical investigation of the hot-cold arrangement in the rows and columns of the zigzag channel shows an 8.6% improvement in the performance of the HX compared to the standard zigzag channel with hot fluid in one channel and cold fluid in another channel [106].

Khan et al. explore the use of PCHE as a compact steam generator for Small Modular Reactors (SMRs). CFD analysis is conducted on a reduced numerical model of the zigzag channel. The geometry is investigated by various bend angles (15°, 25°, 35°, and 45°) and mass fluxes. The Nu increases with the bend angle and mass flux, while the friction factor decreases with Re and increases with the bend angle. The PEC reaches a maximum of 1.45 for a bend angle of 35° and is further enhanced to 1.5 by introducing a 5 mm straight section at each bend angle as depicted in Figure 51 [107]. Wang et al. introduce an improvement in the PCHE channel for $sCO_2$ power cycles by combining straight and

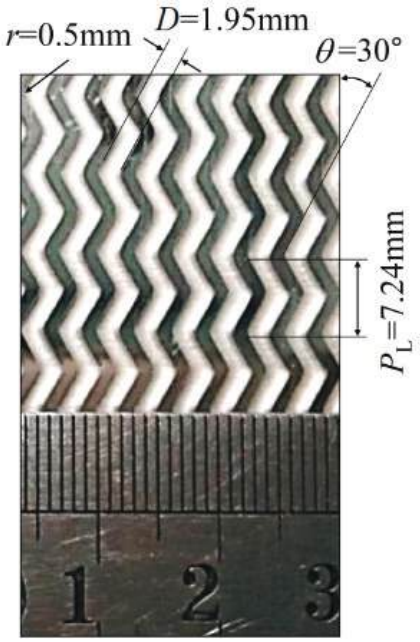


**Figure 48.** Zigzag channels in the PCHE. [From Liu et al. [102], with permission from Elsevier.]

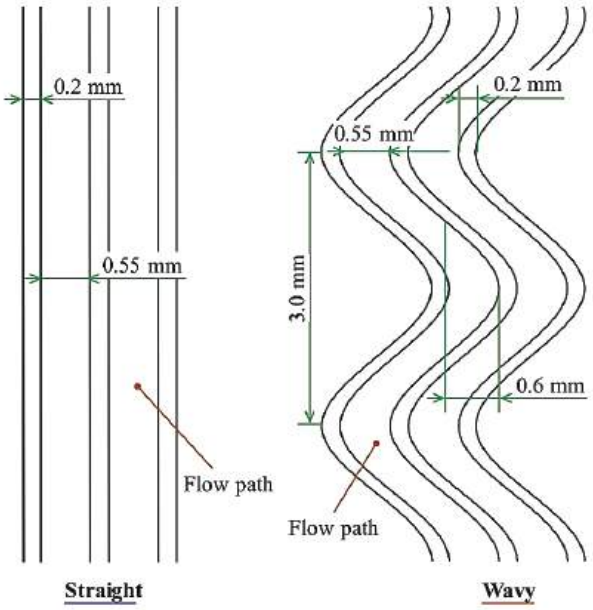


**Figure 49.** Geometric configuration of straight and wavy microchannel designs in PCHE. [From Goto et al. [104], with permission from Elsevier.]

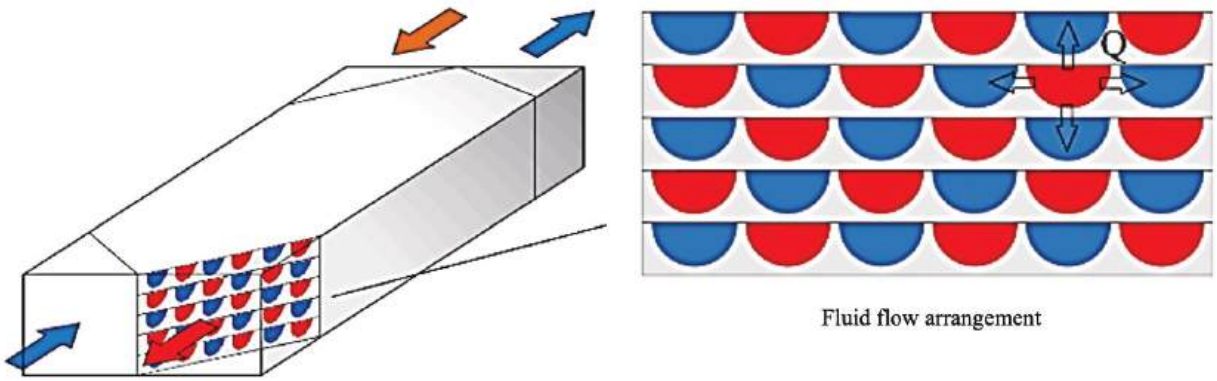


**Figure 50.** Cellular arrangement of zigzag PCHE. [From Liu et al. [106], with permission from Elsevier.]

zigzag channels, as shown in Figure 52. Numerical simulation shows that the friction factor decreases by 33.1% to 84.7%, and the Nu reduction is approximately 3.6% to 30.3% across the range of Re. The modified channel shows a maximum PEC of 45.9% [108]. Liu et al. combine the straight and zigzag channel for LBE and $sCO_2$. The liquid LBE flows in the straight channel and $sCO_2$ in the zigzag channel (Figure 53). The numerical study shows that the combined channel with a 120° zigzag pattern shows higher performance, with a 12.6% increase in heat flux compared to straight channels. The combined channel effectively enhances $sCO_2$ heat transfer, improving overall PCHE performance [109]. Aakre et al. propose a PCHE design with zigzag channels at different angles for molten salt and $sCO_2$ (Figure 54). The molten salt flows through an elliptical channel, closely resembling a circular channel, while $sCO_2$ flows through a semi-circular channel. The molten salt operates in the laminar region, whereas $sCO_2$ operates from laminar to turbulent regions. The new correlations for Nu and friction factor are developed. The friction factor for molten salt is found to be 3 to 5 times higher than the analytical solution for a straight circular channel, and the Nu for molten salt is also higher than that of a straight circular channel [110].

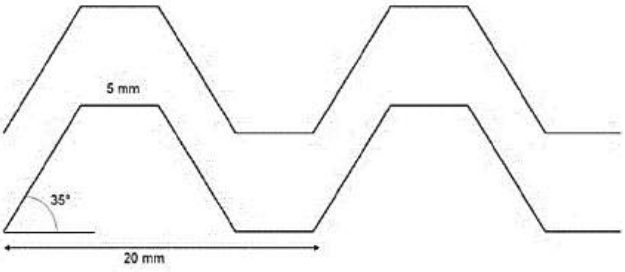


**Figure 51.** Axial profile of zigzag PCHE. [From Khan et al. [107], with permission from Elsevier.]

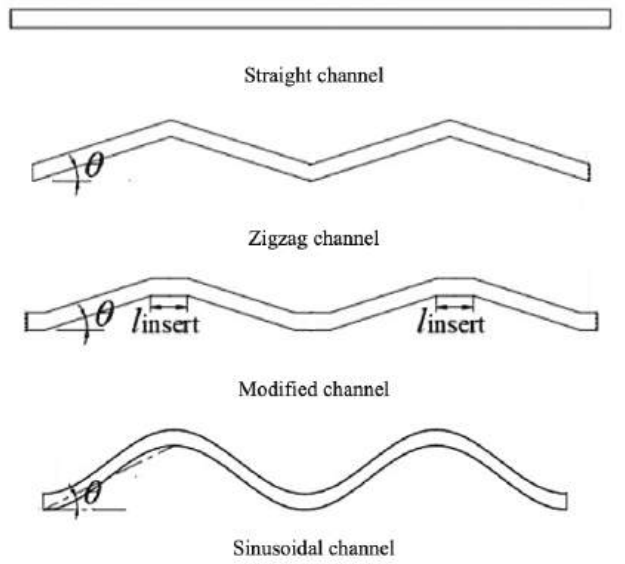


**Figure 52.** Geometric configuration of different types of PCHE. [From Wang et al. [108], with permission from Elsevier.]

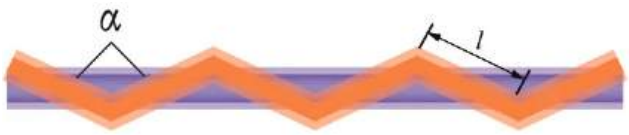


**Figure 53.** Geometric configuration of 120° angle combined channel PCHE. [From Liu et al. [109], with permission from Elsevier.]

Samarmad et al. introduce novel backward/forward-facing wavy channels (BFFWCs) with a 3D flow path design to enhance the performance of PCHE (Figure 55). Numerical simulations and experimental tests are conducted for six BFFWC models to evaluate the Nu, friction factor, effectiveness, and PEC. The results show a maximum of 78% improvement in the Nu for an amplitude (A) of 0.8 and attack angle (Θ) of 60° compared to the straight PCHE. Moreover, the model with A equal to 0.8 and Θ equal to 30° demonstrates the highest PEC of 1.43 [111]. Li et al. perform optimization of A and period (λ) using a multi-objective genetic algorithm for a compact solar receiver in the $sCO_2$ cycle (Figure 56). The result shows optimized design achieves a maximum PEC of 1.21 at a λ of 15.07 mm and an A of 1.73 mm [112]. Samarmad et al. present an innovative two-way corrugated channel having A equal to 0.8 and λ equal to 12.6 (Figure 57). This design results in an improvement of 78% in Nu at the expense of a 130% increase in friction factor. The modified PCHE exhibits a PEC of 1.5 and a 27% improvement in effectiveness [113].

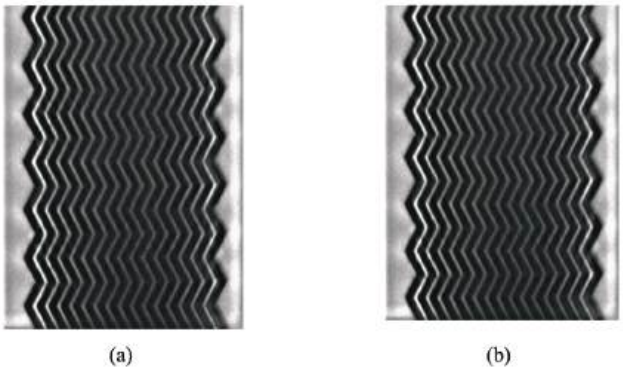


**Figure 54.** Zigzag PCHE: (a) molten salt 30° zigzag channel and (b) $sCO_2$ 37° zigzag channel. [From Aakre et al. [110], with permission from Elsevier.]

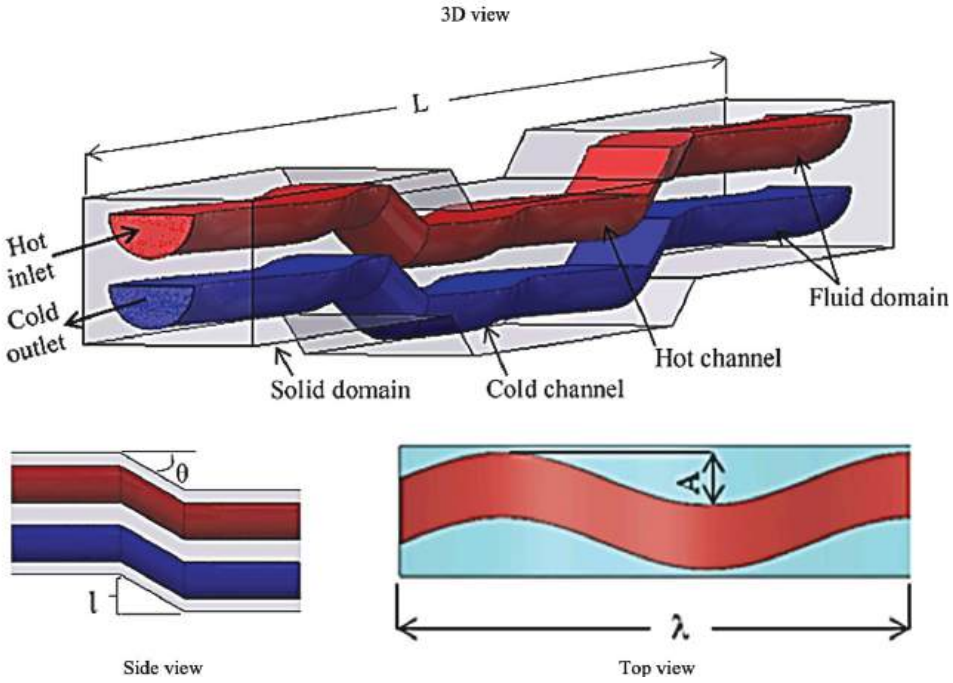


**Figure 55.** Geometric configuration of backward/forward-facing wavy channels PCHE. [From Samarmad et al. [111], with permission from Elsevier.]

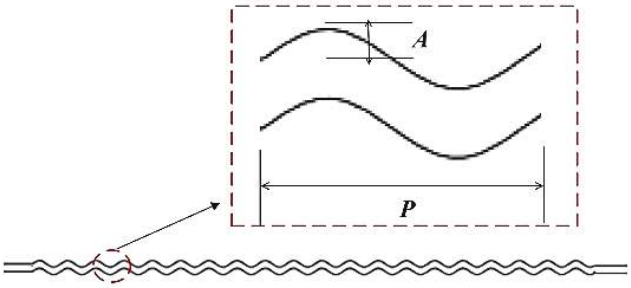


**Figure 56.** Geometric configuration of wavy channel PCHE using amplitude and period. [From Li et al. [112], with permission from Elsevier.]

**Airfoil Channel**

The zigzag designs increase heat transfer but also increase pressure drop up to many folds, as discussed in the previous sub-section. To overcome the higher pressure drop problem airfoil designs are introduced as summarized in Table 10, which show improved heat transfer as compared to a straight channel without increasing the pressure drop like a zigzag channel [114]. Park et al. study the airfoil fin PCHE and compare it with a commercially available zigzag channel PCHE for $sCO_2$ power conversion systems, as shown in Figure 58. Experiments are performed under varying temperatures (70°C to 40.5°C) and pressures (7.5 MPa to 8.5 MPa) conditions. The results show that, for a fixed heat transfer rate to volume ratio, the airfoil design exhibits a 1/5 times lower pressure drop as compared to the zigzag channel [115].

Han et al. study the novel airfoil fins PCHE (Figure 59) and compare it with straight and zigzag channels PCHEs. Under the same operating conditions, the novel airfoil fins display an enhanced overall heat transfer coefficient and reduced pressure drop compared to the straight and zigzag channels. The PEC of the airfoil exhibits an increase of 6.6% to 15.5% and 12.8% to 27.8% compared to the straight and zigzag channels, respectively, over a range of Re [116]. Chung et al. study the airfoil channels for nitrogen ($N_2$) BC recuperator. PEC comparisons show that the airfoil PCHE surpasses straight and zigzag channels, achieving a 21% reduction in volume compared to zigzag PCHE. The airfoil shows the highest PEC of 1.2 at 4000 Re compared to the straight channel PCHE [117].

Li et al. numerically study multiple angles of attack and layouts of airfoils for $sCO_2$ as a working fluid (Figure 60). Airfoil fins with a consistent arrangement transfer more heat than those with an inconsistent arrangement. The performance of the HX decreases with the increase in fin attack angle, with the maximum performance occurring at an attack angle of 15° to 25° [118]. Li et al. study the impact of airfoil fin structural parameters for $sCO_2$ (Figure 61). Increasing the thickness of the airfoil fins ($W_f$) enhances heat transfer but decreases flow characteristics. An increase in the airfoil fins front length ($D_f$) improves both heat transfer and flow characteristics. However, as the front radius of the airfoil fins ($R_f$) increases, the heat transfer and flow characteristics fluctuate. The study recommends the

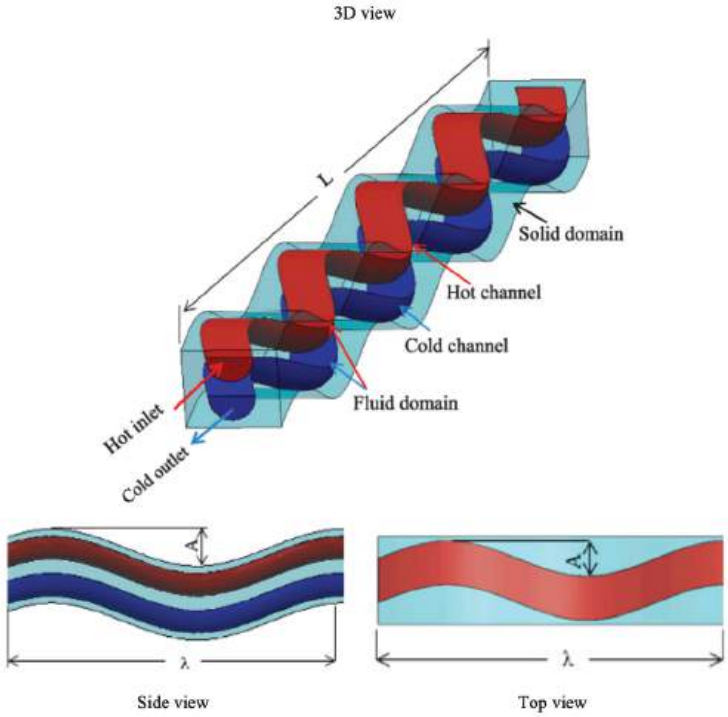


**Figure 57.** Two-way corrugated channels PCHE. [From Samarmad et al. [113], with permission from Elsevier.]

**Table 10.** Heat enhancement using airfoil fins PCHE

| Author | Year | Geometry type | Working fluid | Analysis type | Key findings |
|---|---|---|---|---|---|
| Park et al. [115] | 2024 | Airfoil fin | $sCO_2$ | Experimental | The airfoil fin exhibits a 1/5 times lower pressure drop than that of the zigzag channel. |
| Han et al. [116] | 2023 | Airfoil fins | $sCO_2$ | Experimental and computational | The PEC of the airfoil is 6.6% to 15.5% and 12.8% to 27.8% higher compared to the straight and zigzag channels. |
| Chung et al. [117] | 2023 | Airfoil fin | $N_2$ | Computational | The performance of the airfoil is better than straight PCHE, and zigzag PCHE, and it achieves a 21% reduced volume compared to zigzag PCHE. |
| Li et al. [118] | 2023 | Airfoil channel | $sCO_2$ | Computational | Channels with consistent distributions exhibit enhanced overall performance compared to inconsistent distributions. Airfoil fin angles of 15° to 25° demonstrate the highest performance. |
| Li et al. [119] | 2024 | Airfoil channel | $sCO_2$ | Computational | Increasing airfoil fin thickness improves heat transfer but weakens flow characteristics. Fin-5 ($W_f$=1.5 mm, $D_f$=1.2 & $R_f$=0.26 mm) outperforms Fin-3 ($W_f$=1 mm, $D_f$=1.2 & $R_f$ =0.26 mm) by 2.0–6.3%. |
| Liu et al. [120] | 2024 | Airfoil channel | $sCO_2$ | Computational | The novel DAVG increases the local heat transfer coefficient by up to 120%, outperforming traditional DASVG and NACA0024. |
| Wu et al. [121] | 2023 | Crossed airfoil channel | $sCO_2$ | Computational | Resulting in 25.5% to 30.8% higher Nu and over 10% increase in PEC. |
| Li et al. [122] | 2024 | Airfoil channel | $sCO_2$ | Computational | Integrating airfoil fins with rectangular VGs enhances PEC by 5.95% to 19.47%. |
| Ke et al. [123] | 2023 | Airfoil channel | $sCO_2$ | Computational | Flow-induced pitching of airfoils in rectangular channels results in the highest PEC of 1.4, which is 6% higher than that of active ones. |
| Jin et al. [124] | 2023 | Header with bent channels and airfoils | $sCO_2$ | Computational | The novel header reduces flow non-uniformity by 39.4% and 61.8% at different operating conditions while enhancing overall performance by 5% and 8.5% compared to free and straight channel manifolds. |

following airfoil fin design: $W_f$ =1.5 mm, $D_f$ =1.2 mm & $R_f$ =0.26 mm; $W_f$ =1 mm, $D_f$ =0.6 mm & $R_f$ =0.26 mm and $W_f$ =1 mm, $D_f$ =1.2 mm & $R_f$ =1.46 mm airfoil fin channels, which offer PEC improvements of 2.0% to 6.3%, 0.9% to 5.6%, and 0.13% to 1.81% across the range of Re, respectively, higher than the $W_f$ =1 mm, $D_f$ =1.2 & $R_f$ =0.26 mm airfoil fin channel [119].

Liu et al. study three different airfoil fin PCHE configurations: delta winglet vortex generator (DWVG), delta airfoil vortex generator (DAVG), and delta airfoil staggered vortex generator (DASVG), with NACA0024 airfoil fins as a reference design as shown in Figure 62. The DAVG configurations display a 120% rise in the local heat transfer coefficient [120]. Wu et al. propose a novel crossed airfoil fin design for PCHEs in $sCO_2$ applications (Figure 63). Numerical simulations show that the crossed airfoil fin induces a longitudinal vortex flow, disrupting the flow near the surface and enhancing heat transfer performance. The crossed airfoil fin design demonstrates a 25.5% to 30.8% higher Nu across the range of Re and a 10% increase in the PEC compared to the traditional airfoil fin design [121].

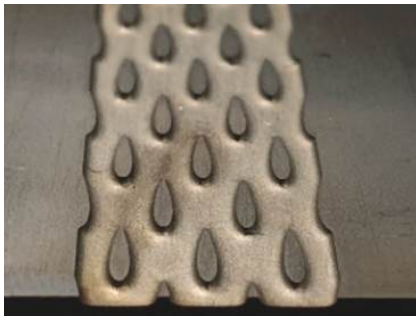

**Figure 58.** Optimized geometric configuration of airfoil fin in the PCHE. [From Park et al. [115], with permission from Elsevier.]

Li et al. combine airfoil fin channels with VG ($H_{VG}$: 0.2 mm, $L_{VG}$: 0.8 mm, and $W_{VG}$: 0.04 mm) as shown in Figure 64. The combined design improves heat transfer, resulting in an increase of 5.95% to 19.47% in PEC compared to conventional airfoil fin channels [122]. Ke et al. study the pitching motion of airfoil fins in a rectangular channel. The study finds that after the Re reached 1000, a self-fluttering of the airfoil fin increases the Nu. The highest PEC of 1.4 is attained when the rotational axis is positioned at 0.42 times the ratio of the elastic axis ($a_x$) to chord length

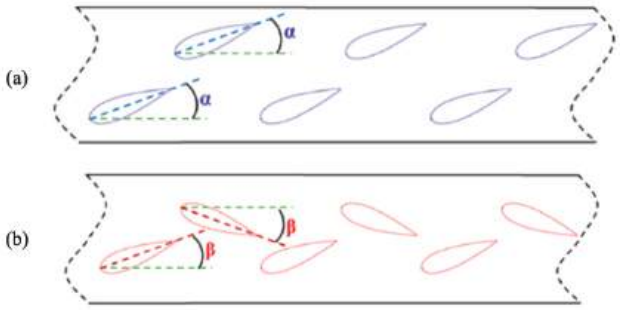


**Figure 60.** Geometric configuration of the airfoil fin PCHE: (a) consistent layout and (b) inconsistent layout. [From Li et al. [118], with permission from Elsevier.]

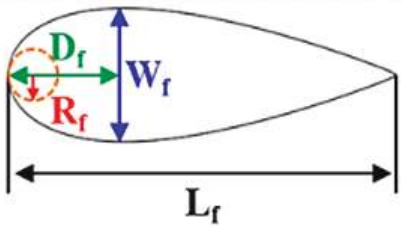


**Figure 61.** Variable parameters of the airfoil fin PCHE. [From Li et al. [119], with permission from Elsevier.]

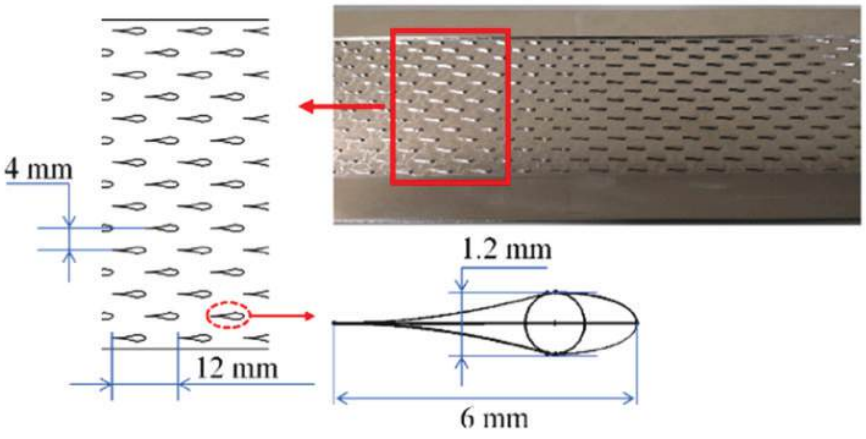


**Figure 59.** Staggered arrangement of airfoil fins in the novel PCHE. [From Han et al. [116], with permission from Elsevier.]

(C) (Figure 65). The passive pitching airfoil shows a 6% higher PEC as compared to the active pitching [123]. Jin et al. propose a new design of the header by combining bent channels and airfoils (Figure 66). The header design reduces flow maldistribution and improves heat transfer characteristics in PCHE channels. The results show that headers with high-pressure drops exhibit uniform fluid distribution in the channels and result in a better heat transfer in the PCHE. The proposed header reduces the flow maldistribution by 39.4% and 61.8% and enhances the performance of the PCHE by 5% and 8.5% compared to the free and straight rib headers, respectively [124].

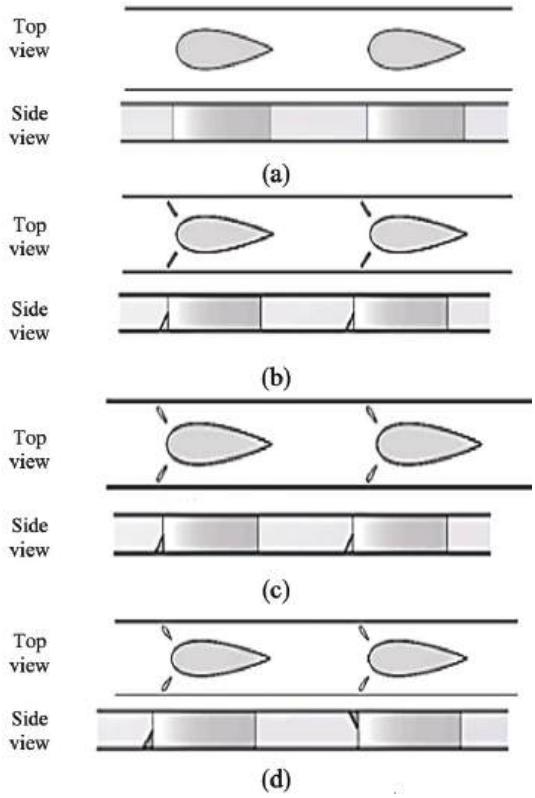


**Figure 62.** Different types of airfoil fin PCHE: (a) NACA0024 airfoil fins, (b) DWVG, (c) DAVG, and (d) DASVG. [From Liu et al. [120], with permission from Elsevier.]

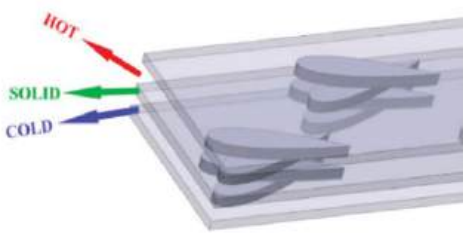


**Figure 63.** Geometric configuration of novel crossed airfoil fin PCHE. [From Wu et al. [121], with permission from Elsevier.]

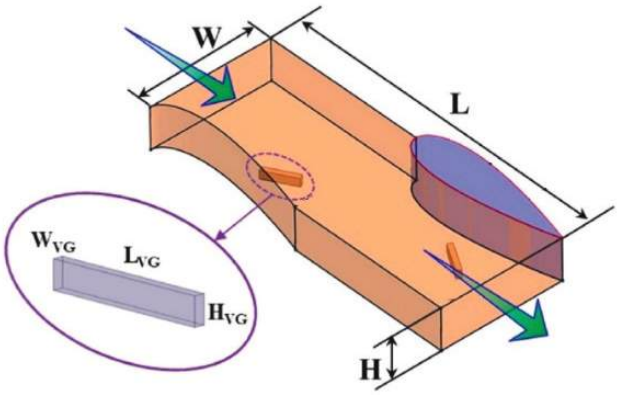


**Figure 64.** Geometric configuration of VG with airfoil fin PCHE. [From Li et al. [122], with permission from Elsevier.]

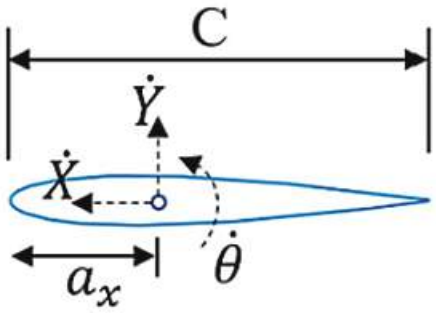


**Figure 65.** Geometric configuration of moving airfoil fin PCHE. [From Ke et al. [123], with permission from Elsevier.]

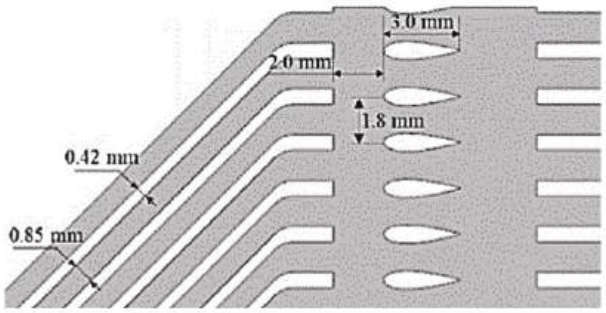


**Figure 66.** Modified manifold with bent fins and airfoil fins for various types of PCHE. [From Jin et al. [124], with permission from Elsevier.]

### Heat Enhancement Using Phase Change Materials

Phase Change Material (PCM) stores and releases thermal energy during phase transitions between solid and liquid states, or vice versa [125]. These materials function like batteries, storing energy and releasing it when needed. PCMs operate based on the latent heat of fusion, making them highly efficient for thermal energy storage [126].

Significant research is currently focused on enhancing heat transfer capabilities and increasing storage capacity, as discussed in Table 11.

Pignata et al. develop a fin tube bundle HX for PCM, using bio-organic PureTemp53 as the PCM placed on the shell side, with heating fluid flowing through the fin tubes (Figure 67). Numerical simulations indicate that reducing the fin pitch from 95 mm to 82 mm increases the heat transfer rate by 34% while increasing the fin height from 20 mm to 32 mm improves the heat transfer rate by 33% [127]. Arqam et al. study paraffin wax as a PCM in a radial fin heat sink for electronic equipment (Figure 68). Experimental and numerical results show that the radial fin design transfers more heat to the PCM, lowers hot surface temperatures, and promotes uniform PCM melting. Increasing the base thickness of the heat sink from 1 mm to 3 mm reduces the heat transfer rate and raises the temperature difference by up to 14.14%. Fin height plays a key role in maintaining uniform flow distribution during PCM melting [128].

Taghavi et al. introduce a plate-type structure for PCM in electronic applications. Numerical simulations demonstrate that the plate-type structure increases energy storage capacity per unit volume by 75% and improves effectiveness by 28.6% compared to a roll-bonded structure (Figure 69) [129]. Abdulateef et al. study a triplex tube HX for thermal energy storage using paraffin with 10% alumina nanoparticles (Figure 70). Optimization studies reveal that using eight fins, with a fin length of 141 mm and a fin aspect ratio

**Table 11.** Heat enhancement using PCM

| Author | Year | Geometry type | Working fluid | Analysis type | Key findings |
|---|---|---|---|---|---|
| Pignata et al. [127] | 2023 | Fin tube HX | Bio-organic | Computational | The pitch and height of the fin change from 95 mm to 82 mm and 20 mm to 32 mm, increases the heat transfer rate by 34% and 33%, respectively. |
| Arqam et al. [128] | 2024 | Radial fin heat sink | Paraffin | Experimental and computational | Fin height is important in maintaining the uniform flow distribution and allowing uniform melting of PCM. |
| Taghavi et al. [129] | 2023 | Plate-type and roll-bounded structure | Paraffin | Experimental and computational | The plate-type structure increases the energy storage capacity per unit volume by 75% and effectiveness by 28.6% than that of the roll-bonded structure. |
| Abdulateef et al. [130] | 2019 | Fin triplex tube HX | Paraffin with 10% alumina nanoparticles | Experimental and computational | The 8 fins, 141 mm fins length, and 18% fins aspect ratio minimize the melting time by 15% and the solidification time by 32.5%. |
| Joybari et al. [131] | 2023 | Pillow plate HX | $CO_2$ | Computational | 25 mm center-to-center aluminum plate displays the best thermal performance with minimum operating cost. |
| Khader et al. [132] | 2024 | Tubular HX | Paraffin and ClimSel C58 | Experimental and computational | The paraffin in HX increases heat discharge time by 438%. Replacing paraffin with ClimSel C58 further increases the storage capacity by 2.35 times. |
| Asgari et al. [133] | 2021 | Branch-shaped fins | Water with hybrid nanofluid ($Al_2O_3$-Cu) 0.04 vol fraction | Computational | The hybrid nanofluid in PCM and a thin fin design show a maximum heat transfer rate. |
| Yazdani et al. [134] | 2022 | Square grid, lightweight HX | Decanoic acid with biochar | Experimental | The 1% addition of biochar increases the energy storage by 32%. |
| Zhang et al. [135] | 2023 | Branch fin design in the triple tube HX | Paraffin with $Al_2O_3$ nanoparticle | Computational | The 2%, 5%, and 8% volume fraction of nanoparticles enhance the heat transfer by 8.5%, 9.3%, and 10.3%. The addition of a branch fin further enhances the heat transfer rate. |
| Fan et al. [136] | 2025 | -- | Mg-Al: PW-EG | Experimental | The 1:3 of Mg-Al: PW-EG brick increases thermal storage efficiency by 95.6%. Replacing paraffin wax with Xylitol and Erythritol further increases the heat storage capacity. |
| Safari et al. [137] | 2024 | Wedge and annular fin | Lauric acid | Experimental | Wedge fin performs 12.8% better transfer heat rate than annular fin tube and 84.3% better than tube HX. |

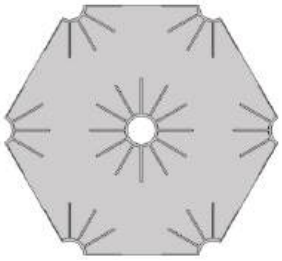

**Figure 67.** Finned tube HX design for PCM. [From Pignata et al. [127], with permission from Elsevier.]

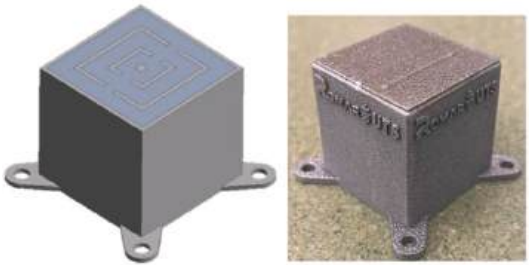

**Figure 68.** Radial fin design for PCM. [From Arqam et al. [128], with permission from Elsevier.]

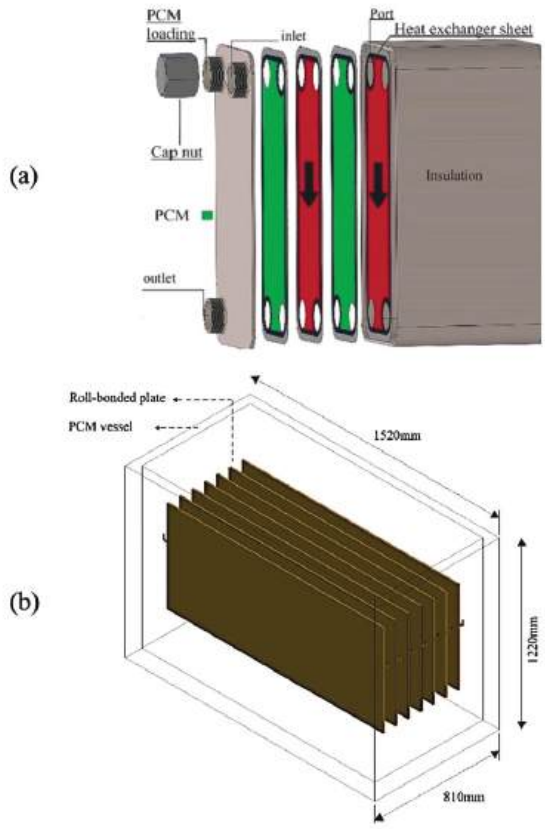


**Figure 69.** Thermal energy storage systems: (a) plate-type and (b) roll-bounded. [From Taghavi et al. [129], with permission from Elsevier.]

of 18%, reduces the melting time from 193 minutes to 163 minutes and the solidification time from 630 minutes to 425 minutes [130]. Joybari et al. develop a pillow plate HX for low-temperature thermal storage applications, using $CO_2$ as the PCM (Figure 71). Numerical simulations show that a 25 mm center-to-center plate distance and aluminum as the construction material provide the best thermal performance at minimal operating costs [131].

Khader et al. propose a novel HX design integrated with PCM (Figure 72). Experimental results show that adding paraffin PCM to the HX increases heat discharge time by 438%. Numerical simulations reveal that replacing paraffin with ClimSel C58 increases storage capacity by 2.35 times [132]. Asgari et al. examine a branch-shaped fin design (Figure 73) combined with a hybrid nanofluid in PCM. Numerical results show that a 0.04 volume fraction of a hybrid nanofluid ($Al_2O_3$-Cu) with a thin fin design maximizes heat transfer [133]. Yazdani et al. design a lightweight square grid HX using a 3D printer (Figure 74). This compact HX uses decanoic acid as PCM. It exhibits a 32% increase in energy storage with a 1% biochar additive. However, further increases in biochar concentration cause particle settlement and reduce heat transfer [134].

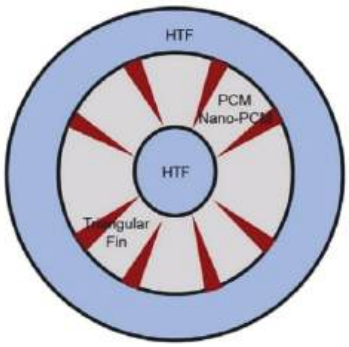


**Figure 70.** Triplex tube HX with heat transfer fluid (HTF) flow channel. [From Abdulateef et al. [130], with permission from Elsevier.]

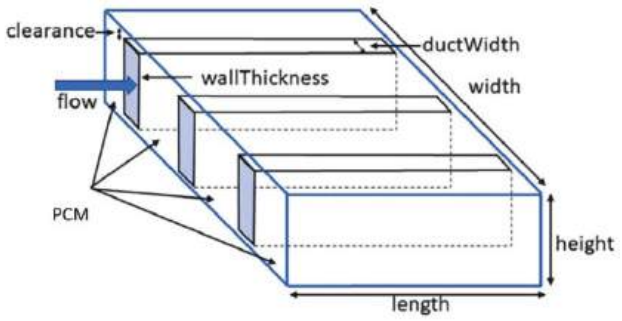


**Figure 71.** Pillow plate HX for the thermal storage application. [From Joybari et al. [131], with permission from Elsevier.]

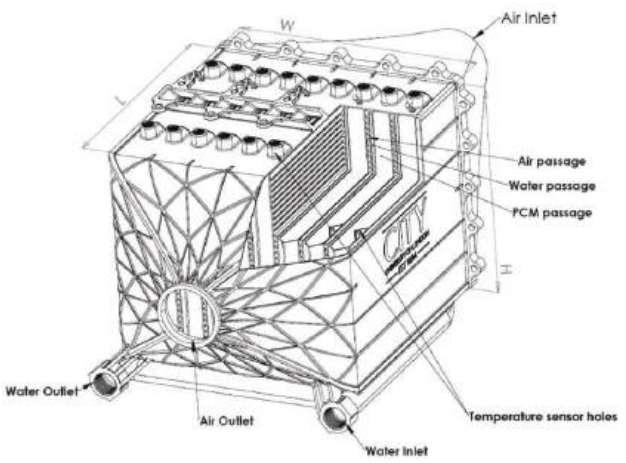


**Figure 72.** HX design integrated with PCM. [From Khader et al. [132], with permission from Elsevier.]

**Figure 74.** Lightweight HX design for thermal storage system. [From Yazdani et al. [134], with permission from Elsevier.]

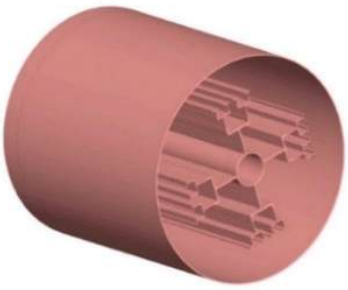

**Figure 73.** Branched shape fin design for PCM. [From Asgari et al. [133], with permission from Elsevier.]

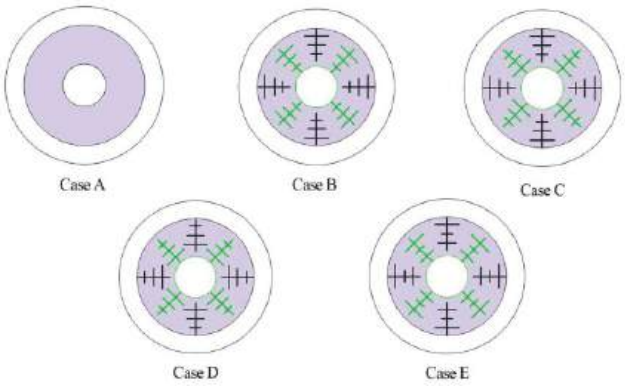


**Figure 75.** Various layouts of branch fin triple tube HX. [From Zhang et al. [135], with permission from Elsevier.]

Zhang et al. introduce a novel branch fin design for a triple tube HX, adding $Al_2O_3$ nanoparticles to paraffin to enhance heat transfer (Figure 75). Numerical simulations indicate that increasing the nanoparticle volume fraction in PCM by 2%, 5%, and 8% enhances heat transfer by 8.5%, 9.3%, and 10.3%, respectively. The branch fin further enhances heat transfer, with cases B, C, D, and E showing 83%, 80.7%, 80.8%, and 82.9% improvements, respectively [135]. Fan et al. combine magnesium-aluminum (Mg-Al) bricks with three different PCMs to enhance thermal storage capacity. Experiments and simulations show that a 1:3 Mg-Al to paraffin wax-expanded graphite (PW-EG) brick configuration improves thermal storage efficiency by 95.6% compared to PW-EG (Figure 76). Replacing paraffin wax with Xylitol and Erythritol further increases the heat storage capacity [136]. Safari et al. propose a novel wedge fin and annular fin HX tube design (Figure 77). Experiments show that the wedge fin tube HX outperforms the annular fin tube HX by 12.8% and the standard tube HX by 84.3% in heat transfer rate [137].

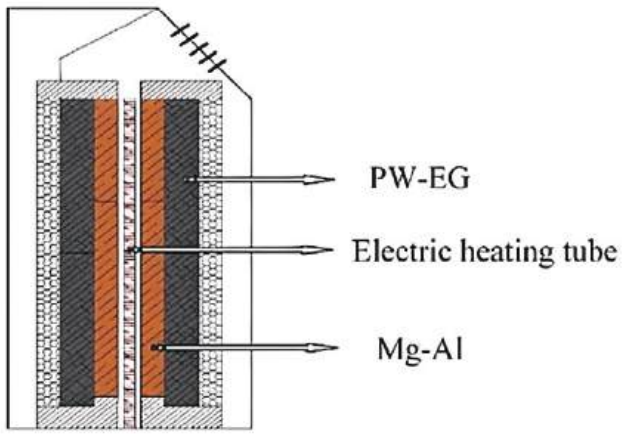


**Figure 76.** Combination of Mg-Al and PW-EG brick for the thermal storage unit. [From Fan et al. [136], with permission from KeAi.].

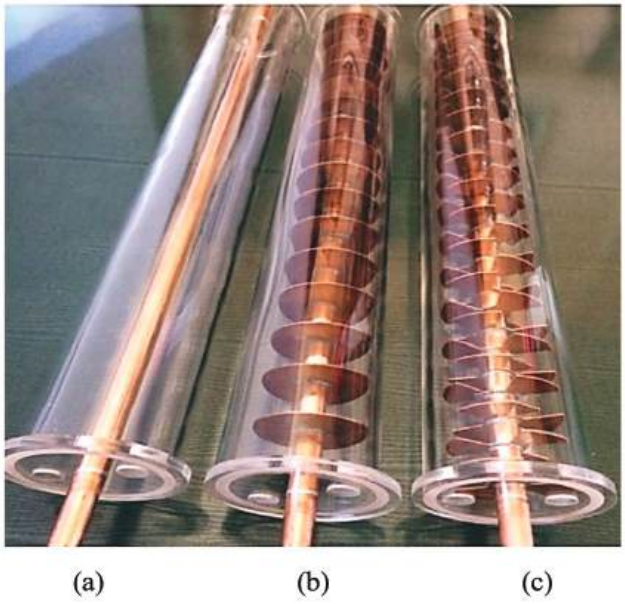


**Figure 77.** Geometric detail of tube HX for PCM: (a) tube HX, (b) annular fin tube HX, and (c) wedge fin tube HX. [From Safari et al. [137], with permission from Elsevier.]

## CONCLUSION

This paper explores the latest advancements in passive heat transfer enhancement techniques specifically designed for power plant applications. The main findings from this review are summarized below:

No single technique is universally better as it highly depends on the specific requirements of the application, including the type of heat exchanger, the fluids properties, and space constraints. However, if we consider the overall effectiveness and flexibility, it is found from this review that gyroid structure, air bubble injection in shell and tube heat exchanger with disc and ring arrangement, v-baffle tubular heat exchanger, and tape insert with trapezoidal geometry are better choices for tubular heat exchangers.

The gyroid structure is very complex and challenging to fabricate. The air bubble injection technique has the highest performance evaluation criteria of 4.5. However, it can't be implemented in most of the applications due to process constraints. V-baffle within a tube has a performance evaluation criteria of 4.07 for air. The Y-shaped tape insert with a trapezoidal configuration has a performance evaluation criteria of 3.68. It is easier to implement in existing and new designs.

The printed circuit heat exchangers offer high heat transfer efficiency, compact design, and suitability for high-pressure and high-temperature applications in advanced nuclear reactors. Printed circuit heat exchangers are prominent in advanced applications requiring compact size and high efficiency, making them a preferred choice for cutting-edge industrial applications and advanced nuclear reactors. The printed circuit heat exchangers with zigzag channels exhibit a 50% enhancement in thermal performance compared to the straight channel.

This comprehensive review of recent advancements in heat transfer techniques covers a wide spectrum of passive heat transfer techniques. It serves as a valuable resource for designers and engineers seeking to optimize heat exchanger designs for specific system requirements. It provides practical insights essential for advancing the next generation of heat exchangers across a wide range of industrial applications. By providing a detailed analysis of various heat enhancement techniques, this paper serves as a key reference point for future research and development of more efficient and effective heat exchanger systems.

## FUTURE DIRECTION

The future of heat exchangers lies in the development of highly efficient, compact, corrosion-resistant, and fouling-resistant designs that can withstand high temperatures and pressures. Achieving this requires focused research and innovation across several key areas. Innovative approaches and technologies are needed to increase the convection heat transfer coefficient, thereby improving the overall efficiency of heat exchangers and ensuring that future designs can operate at peak performance. Additionally, the search for new materials that are more resistant to corrosion, can withstand extreme temperatures and pressures and are robust to thermal shock is essential for extending the lifespan of heat exchangers and reducing maintenance frequency. Advancements in surface treatments and nano-coatings are also crucial, as they improve heat transfer efficiency by maintaining cleaner surfaces over longer periods. Once these issues are addressed, future heat exchangers could meet the demanding requirements of modern industrial applications, paving the way for more efficient, durable, and environmentally friendly thermal management solutions.

## NOMENCLATURE AND ABBREVIATIONS

| | |
|---|---|
| *BC* | *Brayton cycle* |
| *BFFWCs* | *Backward/forward-facing wavy channels* |
| *CFD* | *Computational fluid dynamics* |
| *CFR* | *Coiled flow reverser* |
| *DASVG* | *Delta airfoil staggered vortex generator* |
| *DAVG* | *Delta airfoil vortex generator* |
| *DTTI* | *Dimpled twisted turbulator insert* |
| *DW* | *Deionized water* |
| *DWVG* | *Delta winglet vortex generator* |
| *EG* | *Ethylene glycol* |
| *EHT* | *Eccentrical helical tube* |
| *EMV* | *Electromagnetic vibration* |
| *FPHE* | *Flat plate heat exchanger* |
| *HCW* | *Helical coiled wire* |
| *HCT* | *Helically corrugated tube* |

| | |
|---|---|
| *HTF* | *Heat transfer fluid* |
| *HSHTE* | *Horizontal shell and helically coiled tube exchanger* |
| *HX* | *Heat exchanger* |
| *LBE* | *Lead-bismuth eutectic* |
| *LPM* | *Liter per minute* |
| *Mg-Al* | *Magnesium-aluminum* |
| *MWCNTs* | *Multi-walled carbon nanotubes* |
| $N_2$ | *Nitrogen* |
| *OCT* | *Outward corrugated tube* |
| *PCB* | *Printed circuit board* |
| *PCHE* | *Printed circuit heat exchanger* |
| *PCM* | *Phase Change Material* |
| *PEC* | *Performance evaluation criteria* |
| *PI* | *Perforation indexes* |
| *PTTI* | *Perforated twisted turbulator insert* |
| *PW-EG* | *Paraffin wax-expanded graphite* |
| *PWST* | *Perforated wavy strip turbulator* |
| *RRTT* | *Rectangular-ribbed twisted tape* |
| *RWVG* | *Rectangular winglet vortex generator* |
| $sCO_2$ | *Supercritical carbon dioxide* |
| *SHCHEs* | *Shell and helically coiled heat exchanger* |
| *SMRs* | *Small modular reactors* |
| *SSTT* | *Special shape twisted tape turbulator* |
| *STST* | *Smooth tri-lobed spiral tubes* |
| *TCT* | *Transversely corrugated tube* |
| *TCR* | *Triangular concave rib* |
| *THNFs* | *Tripartite hybrid nanofluids* |
| *TPMS* | *Triply periodic minimal surfaces* |
| *TTI* | *Twisted turbulator insert* |
| *TTT* | *Triangular twisted tape* |
| *TTST* | *Twisted tri-lobed spiral tubes* |
| *TVR* | *Triangular convex rib* |
| *VG* | *Vortex generator* |
| *WST* | *Wavy strip turbulator* |

*Dimensional less number*

| | |
|---|---|
| *Cr* | $C_{p\,min}/\,C_{p\,max}$ |
| *D/H* | *Diameter-to-depth* |
| *e/d* | *Dimensionless height* |
| *Nu* | *Nusselt number* |
| *p/d* | *Dimensionless pitch* |
| *Pr* | *Prandtl number* |
| *Re* | *Reynold number* |

*English Symbol*

| | |
|---|---|
| *A* | *Amplitude (m)* |
| *a* | *Eccentric distance (mm)* |
| $a_x$ | *Elastic axis (mm)* |
| *C* | *Chord length (mm)* |
| *Cp* | *Heat capacity (J/kg.K)* |
| *D* | *Diameter (mm)* |
| $D_f$ | *Leading edge thickness of the airfoil (mm)* |
| *e* | *Eccentricity (mm)* |
| *H* | *Depth (mm)* |
| *h* | *Height (mm)* |
| $H_{VG}$ | *Height of vortex generator (mm)* |
| *L* | *Straight RWVGs length (mm)* |
| $L_{VG}$ | *Length of vortex generator (mm)* |
| $R_f$ | *Radius of the leading edge of the airfoil fins (mm)* |
| *s* | *Pitch (mm)* |
| $W_f$ | *Thickness of the airfoil fins (mm)* |
| *x* | *Longitudinal position of straight RWVGs (mm)* |
| *y* | *Transverse position of straight RWVGs (mm)* |
| *z* | *Offset between tube center and center of curved RWVG (mm)* |

*Greek Symbol*

| | |
|---|---|
| $\Theta$ | *Angle of attack (°)* |
| $\alpha$ | *Arc angle of curved RWVG (°)* |
| $\varphi$ | *Attack angle of straight RWVGs (°)* |
| $\Phi$ | *Concentration of nanoparticle (%age)* |
| $\lambda$ | *Period (mm)* |
| $\Omega$ | *Rotational speed (revolution/ minute)* |

## AUTHORSHIP CONTRIBUTIONS

Authors equally contributed to this work.

## DATA AVAILABILITY STATEMENT

The authors confirm that the data that supports the findings of this study are available within the article. Raw data that support the finding of this study are available from the corresponding author, upon reasonable request.

## CONFLICT OF INTEREST

The author declared no potential conflicts of interest with respect to the research, authorship, and/or publication of this article.

## ETHICS

There are no ethical issues with the publication of this manuscript.

## STATEMENT ON THE USE OF ARTIFICIAL INTELLIGENCE

Artificial intelligence was not used in the preparation of the articl

## REFERENCES

[1] White FM. Viscous fluid flow. New York: McGraw-Hill Inc.; 1991.

[2] Chapman DR. A theoretical analysis of heat transfer in regions of separated flow. NACA-TN-3792; 1956. Available at: https://ntrs.nasa.gov/api/citations/19930084514/downloads/19930084514.pdf. Accessed July 14, 2025.

[3] Picón-Núñez M, Melo-González JC, García-Castillo JL. Use of heat transfer enhancement techniques in the design of heat exchangers. In: Castro Gómez L, Velázquez Flores VM, editors. Advances in heat exchangers. London: IntechOpen; 2022.
[4] Kumar KS, Muniamuthu S, Mohan KR. Measurement of temperature flow analysis by condition monitoring system for WTG gear box to evaluate the thermal performance associated with plant load factor. J Therm Eng 2023;9:979−987. [CrossRef]
[5] Roy U, Roy PK. Advances in heat intensification techniques in shell and tube heat exchanger. In: Advanced analytic and control techniques for thermal systems with heat exchangers. Cambridge: Academic Press; 2020. p. 197−207. [CrossRef]
[6] Varuvel EG, Sonthalia A, Aloui F, Saravanan CG. Basics of heat transfer: Heat exchanger. In: Handbook of thermal management systems. Amsterdam: Elsevier; 2023. p. 79−93. [CrossRef]
[7] Babaelahi M, Babazadeh MA, Saadatfar M. New design for the cold part of heat pipes using functionally graded material in heat sink with variable thickness fins: An analytical approach. J Therm Eng 2024;10:1323−1334. [CrossRef]
[8] Hasan KS, Al-fahham M, Abd Al-wahid WA, Khwayyir HH, Kareem AR, Hasan SS, Al-naffakh J. Experimental study on the combustion of gaseous based fuel (LPG) in a tangential swirl burner of a steam boiler. J Therm Eng 2024;10:1226−1240. [CrossRef]
[9] Deshmukh MS, Deshmukh DS, Chavhan SP. A critical assessment of the implementation of phase change materials in the VCC of refrigerator. J Therm Eng 2022;8:562−572. [CrossRef]
[10] Anderson Process. A Closer Look at Heat Exchangers. Available at: https://www.anderson-process.com/a-closer-look-at-heat-exchangers/. Accessed July 14, 2025.
[11] Kılıc M, Ullah A. Numerical investigation of effect of different parameter on heat transfer for a cross-flow heat exchanger by using nanofluids. J Therm Eng 2021;7:1980−1989. [CrossRef]
[12] Li H, Wang Y, Han Y, Li W, Yang L, Guo J, Jiang F. A comprehensive review of heat transfer enhancement and flow characteristics in the concentric pipe heat exchanger. Powder Technol 2022;397:117037. [CrossRef]
[13] Tavousi E, Perera N, Flynn D, Hasan R. Heat transfer and fluid flow characteristics of the passive method in double tube heat exchangers: A critical review. Int J Thermofluids 2023;17:100282. [CrossRef]
[14] Liu S, Sakr M. A comprehensive review on passive heat transfer enhancements in pipe exchangers. Renew Sustain Energy Rev 2013;19:64−81. [CrossRef]
[15] Zhang J, Zhu X, Mondejar ME, Haglind F. A review of heat transfer enhancement techniques in plate heat exchangers. Renew Sustain Energy Rev 2019;101:305−328. [CrossRef]
[16] Alam T, Kim MH. A comprehensive review on single phase heat transfer enhancement techniques in heat exchanger applications. Renew Sustain Energy Rev 2018;81:813−839. [CrossRef]
[17] Mousa MH, Miljkovic N, Nawaz K. Review of heat transfer enhancement techniques for single phase flows. Renew Sustain Energy Rev 2021;137:110566. [CrossRef]
[18] Mousa MH, Yang CM, Nawaz K, Miljkovic N. Review of heat transfer enhancement techniques in two-phase flows for highly efficient and sustainable cooling. Renew Sustain Energy Rev 2022;155:111896. [CrossRef]
[19] Diaconu BM, Cruceru M, Anghelescu L. A critical review on heat transfer enhancement techniques in latent heat storage systems based on phase change materials. Passive and active techniques, system designs and optimization. J Energy Storage 2023;61:106830. [CrossRef]
[20] Bdaiwi M, Akroot A, Wahhab HAA, Assaf YH, Nawaf MY, Talal W. Enhancement heat exchanger performance by insert dimple surface ball inside tubes: A review. Results Eng 2023;19:101323. [CrossRef]
[21] Bhatnagar MK, Rai M, Ashraf M, Kapoor O, Mamatha TG, Vishnoi M. Efficiency enhancement of heat exchanger using inserts and nano-fluid: A review. Mater Today Proc 2021;44:4399−4403. [CrossRef]
[22] Habibishandiz M, Saghir MZ. A critical review of heat transfer enhancement methods in the presence of porous media, nanofluids, and microorganisms. Therm Sci Eng Prog 2022;30:101267. [CrossRef]
[23] Ho MLG, Oon CS, Tan LL, Wang Y, Hung YM. A review on nanofluids coupled with extended surfaces for heat transfer enhancement. Results Eng 2023;17:100957. [CrossRef]
[24] Khargotra R, Kumar R, Nadda R, Dhingra S, Alam T, Dobrota D, et al. RETRACTED: A review of different twisted tape configurations used in heat exchanger and their impact on thermal performance of the system. Heliyon 2023;9:e16390. [CrossRef]
[25] Shelare SD, Aglawe KR, Belkhode PN. A review on twisted tape inserts for enhancing the heat transfer. Mater Today Proc 2022;54:560−565. [CrossRef]
[26] Li W, Yu Z. Heat exchangers for cooling supercritical carbon dioxide and heat transfer enhancement: A review and assessment. Energy Rep 2021;7:4085−4105. [CrossRef]
[27] Nguyen DH, Ahn HS. A comprehensive review on micro/nanoscale surface modification techniques for heat transfer enhancement in heat exchanger. Int J Heat Mass Transf 2021;178:121601. [CrossRef]
[28] Sheikholeslami M, Gorji-Bandpy M, Ganji DD. Review of heat transfer enhancement methods: Focus on passive methods using swirl flow devices. Renew Sustain Energy Rev 2015;49:444−469. [CrossRef]

[29] Ahmed W, Zhan Y, Zhang H, Zhou X, Shahid M, Mudasar F, et al. Preparation, applications, stability and improved thermal characteristics of sonochemically synthesized nanosuspension using varying heat exchangers: A review. J Mol Liq 2023;387:122665. [CrossRef]
[30] Sadique H, Murtaza Q. Heat transfer augmentation in microchannel heat sink using secondary flows: A review. Int J Heat Mass Transf 2022;194:123063. [CrossRef]
[31] Ali MR, Al-Khaled K, Hussain M, Labidi T, Khan SU, Kolsi L, et al. Effect of design parameters on passive control of heat transfer enhancement phenomenon in heat exchangers: A brief review. Case Stud Therm Eng 2023;43:102674. [CrossRef]
[32] Babu R, Kumar P, Roy S, Ganesan R. A comprehensive review on compound heat transfer enhancement using passive techniques in a heat exchanger. Mater Today Proc 2022;54:428–436. [CrossRef]
[33] Hughes MT, Garimella S. A review of active enhancement methods for boiling and condensation. Int J Heat Mass Transf 2024;218:124752. [CrossRef]
[34] Dehbani M, Rahimi M, Rahimi Z. A review on convective heat transfer enhancement using ultrasound. Appl Therm Eng 2022;208:118273. [CrossRef]
[35] Mousavi Ajarostaghi SS, Zaboli M, Javadi H, Badenes B, Urchueguia JF. A review of recent passive heat transfer enhancement methods. Energies 2022;15:986. [CrossRef]
[36] Lu Q, Liu Y, Deng J, Luo X, Deng Z, Mi Z. Review of interdisciplinary heat transfer enhancement technology for nuclear reactor. Ann Nucl Energy 2021;159:108302. [CrossRef]
[37] Gugulothu R, Reddy KVK, Somanchi NS, Adithya EL. A review on enhancement of heat transfer techniques. Mater Today Proc 2017;4:1051–1056. [CrossRef]
[38] Edreis E, Petrov A. Types of heat exchangers in industry, their advantages and disadvantages, and the study of their parameters. In: IOP Conf Ser Mater Sci Eng 2020;963:012027. [CrossRef]
[39] Khan MA, Khalid MD, Ilyas M, Nauman MD, Asim M, Waheed K, et al. Experimental and numerical study of an innovative twined tube HX design. Ann Nucl Energy 2024;195:110185. [CrossRef]
[40] Li C, Hou J, Wang Y, Wei S, Zhou P, He Z, et al. Dynamic heat transfer characteristics of ice storage in smooth-tube and corrugated-tube heat exchangers. Appl Therm Eng 2023;223:120037. [CrossRef]
[41] Qin SY, Yu ZQ, Fang ZB, Liu W, Shan F. Effects of the wall heat flux on the flow characteristics of large-scale coherent structures in a pipe with enhanced heat transfer. Chem Eng Sci 2023;282:119284. [CrossRef]
[42] Hu Q, Qu X, Peng W, Wang J. Experimental and numerical investigation of turbulent heat transfer enhancement of an intermediate heat exchanger using corrugated tubes. Int J Heat Mass Transf 2022;185:122385. [CrossRef]
[43] Rezaei A, Hadibafekr S, Khalilian M, Chitsaz A, Mirzaee I, Shirvani H. A comprehensive numerical study on using lobed cross-sections in spiral heat exchanger: Fluid flow and heat transfer analysis. Int J Therm Sci 2023;193:108464. [CrossRef]
[44] Khashaei A, Ameri M, Azizifar S, Cheraghi MH. Experimental investigation on the heat transfer augmentation and friction factor inside tube enhanced with deep dimples. Int Commun Heat Mass Transf 2023;149:107149. [CrossRef]
[45] Xin F, Wu H, Sun Y, Zhang J, Yang Y, Zhao B. Numerical simulation study of heat transfer enhancement in a tube based on an eccentric structure. Energy Rep 2023;9:275–283. [CrossRef]
[46] Li W, Yu Z. Heat transfer enhancement of supercritical carbon dioxide in eccentrical helical tubes. Int J Heat Mass Transf 2024;221:125041. [CrossRef]
[47] Islam MS, Saha SC. Heat transfer enhancement investigation in a novel flat plate heat exchanger. Int J Therm Sci 2021;161:106763. [CrossRef]
[48] Yahiat F, Bouvier P, Russeil S, André C, Bougeard D. Swirl influence on thermo-hydraulic performances within a heat exchanger/reactor with macro deformed walls in laminar flow regime. Chem Eng Process Process Intensif 2023;189:109373. [CrossRef]
[49] Zhao J, Reda SA, Al-Zahrani KS, Singh PK, Amin MT, Tag-Eldin E, Emami F. Hydro-thermal and economic analyses of the air/water two-phase flow in a double tube heat exchanger equipped with wavy strip turbulator. Case Stud Therm Eng 2022;37:102260. [CrossRef]
[50] Luo J, Asadollahzadeh M, Chauhan BS, Abdalmonem A, Elbadawy I, Salah B, et al. First and second law analysis of a heat exchanger equipped with perforated wavy strip turbulator in the presence of water-CuO nanofluid. Case Stud Therm Eng 2024;54:103968. [CrossRef]
[51] Wang N, Ghoushchi SP, Sharma K, Elbadawy I, Mouldi A, Loukil H, et al. Thermal performance enhancement in a double tube heat exchanger using combination of bubble injection and helical coiled wire insert. Case Stud Therm Eng 2023;52:103722. [CrossRef]
[52] Al-darraji AR, Marzouk SA, Aljabr A, Almehmadi FA, Alqaed S, Kaood A, et al. Enhancement of heat transfer in a vertical shell and tube heat exchanger using air injection and new baffles: Experimental and numerical approach. Appl Therm Eng 2024;236:121493. [CrossRef]
[53] Zhou X, Bai H, Xu Q, Mansir IB, Ayed H, Abbas SZ, et al. Evaluations on effect of volume fraction of injected air on exergo-economic performance of a shell and tube heat exchanger. Case Stud Therm Eng 2022;35:101919. [CrossRef]
[54] Rastan H, Abdi A, Hamawandi B, Ignatowicz M, Meyer JP, Palm B, et al. Heat transfer study of enhanced additively manufactured minichannel heat exchangers. Int J Heat Mass Transf 2020;161:120271. [CrossRef]

[55] Aridi R, Ali S, Lemenand T, Faraj J, Khaled M. CFD analysis on the spatial effect of vortex generators in concentric tube heat exchangers: A comparative study. Int J Thermofluids 2022;16:100247. [CrossRef]
[56] Hassan JH, Hameed VM. Evaluate the hydro-thermal behavior in the heat exchanger equipped with an innovative turbulator. S Afr J Chem Eng 2022;41:182–192. [CrossRef]
[57] Vahidifar S, Banihashemi S. Experimental and numerical evaluation of heat transfer enhancement by internal flow excitation. Int J Therm Sci 2023;192:108395. [CrossRef]
[58] Salhi JE, Zarrouk T, Merrouni AA, Salhi M, Salhi N. Numerical investigations of the impact of a novel turbulator configuration on the performances enhancement of heat exchangers. J Energy Storage 2022;46:103813. [CrossRef]
[59] Zhu S, Li L, Qi T, Hu W, Cheng C, Cao S, et al. The effect of swallow-shaped bionic ribs on the thermal-hydraulic performance of heat exchanger tubes. Therm Sci Eng Prog 2023;46:102180. [CrossRef]
[60] Zhao L, Qian Z, Wang X, Wang Q, Li C, Zhang Z, et al. Analysis of the thermal improvement of plate fin-tube heat exchanger with straight and curved rectangular winglet vortex generators. Case Stud Therm Eng 2023;51:103612. [CrossRef]
[61] Dadvand A, Hosseini S, Aghebatandish S, Khoo BC. Enhancement of heat and mass transfer in a microchannel via passive oscillation of a flexible vortex generator. Chem Eng Sci 2019;207:556–580. [CrossRef]
[62] Mousavi SMS, Alavi SMA. Experimental and numerical study to optimize flow and heat transfer of airfoil-shaped turbulators in a double-pipe heat exchanger. Appl Therm Eng 2022;215:118961. [CrossRef]
[63] Vishwakarma DK, Bhattacharyya S, Soni MK, Goel V, Meyer JP. Evaluating the heat transfer and pressure drop in the transitional flow regime for a horizontal circular tube fitted with wavy-tape inserts. Int J Therm Sci 2024;196:108677. [CrossRef]
[64] Farnam M, Khoshvaght-Aliabadi M, Asadollahzadeh MJ. Heat transfer intensification of agitated U-tube heat exchanger using twisted-tube and twisted-tape as passive techniques. Chem Eng Process Process Intensif 2018;133:137–147. [CrossRef]
[65] Luo J, Alghamdi A, Aldawi F, Moria H, Mouldi A, Loukil H, et al. Thermal-frictional behavior of new special shape twisted tape and helical coiled wire turbulators in engine heat exchangers system. Case Stud Therm Eng 2024;53:103877. [CrossRef]
[66] Forooghi P, Flory M, Bertsche D, Wetzel T, Frohnapfel B. Heat transfer enhancement on the liquid side of an industrially designed flat-tube heat exchanger with passive inserts: Numerical investigation. Appl Therm Eng 2017;123:573–583. [CrossRef]
[67] Heeraman J, Kumar R, Chaurasiya PK, Beloev HI, Iliev IK. Experimental evaluation and thermal performance analysis of a twisted tape with dimple configuration in a heat exchanger. Case Stud Therm Eng 2023;46:103003. [CrossRef]
[68] Farhadi S, Shekari Y, Omidvar P. Numerical and experimental investigation of laminar and turbulent convective heat transfer in a coiled flow reverser with twisted tape insert. Int J Therm Sci 2024;197:108781. [CrossRef]
[69] Ifraj NF, Fahad MK, Tahsin SH, Haque MR, Haque MM. Numerical investigation of the thermal performance optimization inside a heat exchanger tube using different novel combination of perforations on Y-shaped insert. Int J Therm Sci 2023;194:108583. [CrossRef]
[70] Gnanavel C, Saravanan R, Chandrasekaran M. Heat transfer enhancement through nano-fluids and twisted tape insert with rectangular cut on its rib in a double pipe heat exchanger. Mater Today Proc 2020;21:865–869. [CrossRef]
[71] Azhari AA, Milyani AH, Abu-Hamdeh NH, Hussin AM. Thermal improvement of heat exchanger with involve of swirl flow device utilizing nanomaterial. Case Stud Therm Eng 2023;44:102793. [CrossRef]
[72] Saini R, Gupta B, Shukla AP, Singh B, Baredar P, Bisen A, et al. CFD analysis of heat transfer enhancement in a concentric tube counter flow heat exchanger using nanofluids ($SiO_2/H_2O$, $Al_2O_3/H_2O$, $CNTs/H_2O$) and twisted tape turbulators. Mater Today Proc 2023;76:418–429. [CrossRef]
[73] Kumar V, Sahoo RR. 4 E's (energy, exergy, economic, environmental) performance analysis of air heat exchanger equipped with various twisted turbulator inserts utilizing ternary hybrid nanofluids. Alex Eng J 2022;61:5033–5050. [CrossRef]
[74] Das L, Aslfattahi N, Habib K, Saidur R, Das A, Kadirgama K, et al. Thermohydraulic performance investigation of a heat exchanger with combined effect of ribbed insert and Therminol55/MXene+$Al_2O_3$ nanofluid: A numerical two-phase approach. Heliyon 2023;9:e14283. [CrossRef]
[75] Nguyen DH, Nguyen PQ, Rehman RU, Kim JF, Ahn HS. Optimizing the effect of micro-surface on the thermal hydraulic performance of plate heat exchanger. Appl Therm Eng 2024;239:122172. [CrossRef]
[76] Khalaf-Allah RA, Mohamed SM, Saeed E, Tolan M. Augmentation of water pool boiling heat transfer using heating surfaces fabricated by multi passive techniques. Appl Therm Eng 2023;219:119693. [CrossRef]
[77] Moharana S, Das M, Pecherkin N, Pavlenko A, Volodin O. Experimental assessment of enhanced 2×3 semi-closed microstructure tube bundle as an alternative in shell and tube heat exchangers. Appl Therm Eng 2023;232:120966. [CrossRef]

[78] Alnaimat F, AlHamad IM, Mathew B. Heat transfer intensification in MEMS two-fluid parallel flow heat exchangers by embedding pin fins in microchannels. Int J Thermofluids 2021;9:100048. [CrossRef]
[79] Dizjeh SZ, Brinkerhoff J. Numerical investigations of turbulent heat transfer enhancement in circular tubes via modified internal profiles. Int J Thermofluids 2022;16:100237. [CrossRef]
[80] Alteneiji M, Ali MIH, Khan KA, Al-Rub RKA. Heat transfer effectiveness characteristics maps for additively manufactured TPMS compact heat exchangers. Energy Storage Saving 2022;1:153–161. [CrossRef]
[81] Yan K, Deng H, Xiao Y, Wang J, Luo Y. Thermo-hydraulic performance evaluation through experiment and simulation of additive manufactured Gyroid-structured heat exchanger. Appl Therm Eng 2024;241:122402. [CrossRef]
[82] Liu M, Calautit JK. A parametric investigation of the heat transfer enhancement of tube bank heat exchanger with reversed trapezoidal profile fins. Therm Sci Eng Prog 2023;42:101914. [CrossRef]
[83] Soheibi H, Shomali Z, Ghazanfarian J. Combined active-passive heat transfer control using slotted fins and oscillation: The cases of single cylinder and tube bank. Int J Heat Mass Transf 2022;182:121972. [CrossRef]
[84] Searle M, Ramesh S, Straub D. Optimization-inspired pin-fin array for supercritical carbon dioxide recuperator. Appl Therm Eng 2024;241:122335. [CrossRef]
[85] Tariq H, Sajjad R, Khan MZU, Ghachem K, Naqvi AA, Khan SU, et al. Effective waste heat recovery from engine exhaust using fin prolonged heat exchanger with graphene oxide nanoparticles. J Indian Chem Soc 2023;100:100911. [CrossRef]
[86] Marzouk SA, Abou Al-Sood MM, El-Said EM, Younes MM, El-Fakharany MK. A comprehensive review of methods of heat transfer enhancement in shell and tube heat exchangers. J Therm Anal Calorim 2023;148:7539–7578. [CrossRef]
[87] Mazharmanesh S, Tian FB, Lei C. Enhancing heat transfer using flow-induced oscillations of a flexible baffle attached to a vertical heated flat surface. Int J Therm Sci 2023;194:108604. [CrossRef]
[88] Boonloi A, Jedsadaratanachai W. Flow and heat transfer profiles in a heat exchanger tube equipped with XV baffles (XVB): A numerical analysis. Case Stud Therm Eng 2023;49:103263. [CrossRef]
[89] Rahman MA, Dhiman SK. Performance evaluation of turbulent circular heat exchanger with a novel flow deflector-type baffle plate. J Eng Res 2024;12:941–949. [CrossRef]
[90] Abidi A, Sajadi SM. Numerical assessment of hydraulic behavior and thermal efficiency of multiphase hybrid nanofluid in a shell-and-tube heat exchanger with inclined baffles. Eng Anal Bound Elem 2023;156:114–125. [CrossRef]
[91] Ma Y, Xie G, Hooman K. Review of printed circuit heat exchangers and its applications in solar thermal energy. Renew Sustain Energy Rev 2022;155:111933. [CrossRef]
[92] Pandey V, Kumar P. Modelling and analysis of precooler for a sCO2 Brayton cycle with different banking configurations using a stack-based model. Appl Therm Eng 2024;242:122466. [CrossRef]
[93] Zhong SG, Ren Y, Wang PD, Wu WD, Yang YY, Yang QG. Experimental test of rectangular microchannel printed circuit heat exchanger using supercritical carbon dioxide as working fluid. J Supercrit Fluids 2023;200:105967. [CrossRef]
[94] Xu P, Zhou T, Fu Z, Mao S, Chen J, Jiang Y. Heat transfer performance of liquid lead–bismuth eutectic and supercritical carbon dioxide in double D-type straight channel. Appl Therm Eng 2023;219:119484. [CrossRef]
[95] Li X, Su X, Gu L, Liu D, Wang G, Wang X, Guo Y. Investigation on thermo-hydraulic characteristic of lead–bismuth eutectic and supercritical carbon dioxide in a straight-channel printed circuit heat exchanger. Appl Therm Eng 2024;240:122294. [CrossRef]
[96] Li Q, Lin ZJ, Yang L, Wang Y, Li Y, Cai WH. Micro segment analysis of supercritical methane thermal-hydraulic performance and pseudo-boiling in a PCHE straight channel. Pet Sci 2024;21:1275–1289. [CrossRef]
[97] Xu J, Ma Y, Han Z, Wang Q, Ma T. Thermal design of printed circuit heat exchanger used for lead-bismuth fast reactor. Appl Therm Eng 2023;226:120343. [CrossRef]
[98] Lee G, Joo Y, Yu Y, Kim HG. Dual-fluid topology optimization of printed-circuit heat exchanger with low-pumping-power design. Case Stud Therm Eng 2023;49:103318. [CrossRef]
[99] Tong ZX, Zou TT, Jiang T, Yang JQ. Investigation of field synergy principle for convective heat transfer with temperature-dependent fluid properties. Case Stud Therm Eng 2023;45:102926. [CrossRef]
[100] Lao J, Ding J, Fu Q, Wang W, Lu J. Heat transfer between molten salt and supercritical CO2 in discontinuous fins print circuits heat exchanger. Energy Procedia 2019;158:5832–5837. [CrossRef]
[101] He M, Talaat K, Chen M. Design and optimization of molten salt printed circuit steam generators. Appl Therm Eng 2024;238:122161. [CrossRef]
[102] Liu SH, Liu RL, Huang YP, Zhu XL, Yang L, Tang J, et al. Experimental study on flow and heat transfer of supercritical carbon dioxide in zigzag channels with bending angle 30° for advanced nuclear systems. Ann Nucl Energy 2023;185:109720. [CrossRef]
[103] Saeed M, Berrouk AS, Al Wahedi YF, Alam K, Singh MP, Siddiqui MS, et al. A machine learning-based study of sCO2 cycle precooler's design and performance with straight and zigzag channels. Appl Therm Eng 2024;236:121522. [CrossRef]

[104] Goto T, Jige D, Inoue N, Sagawa K. Condensation flow visualization, heat transfer, and pressure drop in printed circuit heat exchangers with straight and wavy microchannels. Int J Refrig 2023;152:234–240. [CrossRef]
[105] Ahmed MM, Ehsan MM. Design and off-design performance analysis of a zigzag channeled precooler for indirect cooling system of supercritical CO2 recompression cycle incorporated with a flow-bypass system. Appl Therm Eng 2023;226:120321. [CrossRef]
[106] Liu S, Gao C, Liu M, Chen Y, Tang J, Huang Y, et al. An improved zigzag-type printed circuit heat exchanger for supercritical CO2 Brayton cycles. Ann Nucl Energy 2023;183:109653. [CrossRef]
[107] Khan MA, Sohail SA, Waheed K, Siddique W, Ilyas M, Aydogan F, et al. Numerical investigation of thermal-hydraulic design of a printed circuit steam generator. Ann Nucl Energy 2023;186:109736. [CrossRef]
[108] Wang J, Yan XP, Boersma BJ, Lu MJ, Liu X. Numerical investigation on the thermal-hydraulic performance of the modified channel supercritical CO2 printed circuit heat exchanger. Appl Therm Eng 2023;221:119678. [CrossRef]
[109] Liu H, Zhang Z, Yang S, Chen G, Cong T, Du H. Numerical investigation on flow and heat transfer characteristics of a PCHE with liquid lead–bismuth eutectic and sCO2 as working fluids. Ann Nucl Energy 2024;200:110367. [CrossRef]
[110] Aakre SR, Anderson MH. Pressure drop and heat transfer characteristics of nitrate salt and supercritical CO2 in a diffusion-bonded heat exchanger. Int J Heat Mass Transf 2022;189:122691. [CrossRef]
[111] Samarmad AO, Jaffal HM. Examining the effect of backward/forward-facing wavy channels on the thermohydraulic performance of a printed circuit heat exchanger under the laminar flow regime. Int J Thermofluids 2023;20:100485. [CrossRef]
[112] Li XL, Li YF, Zhang ZD, Fan YH, Wang JY, Wang K, et al. Optimization of a wavy-channel compact solar receiver with supercritical carbon dioxide. Appl Therm Eng 2024;241:122373. [CrossRef]
[113] Samarmad AO, Jaffal HM. Performance evaluation of a printed circuit heat exchanger with a novel two-way corrugated channel. Results Eng 2023;19:101303. [CrossRef]
[114] Tu Y, Zeng Y. Numerical study on flow and heat transfer characteristics of supercritical CO2 in zigzag microchannels. Energies 2022;15:2099. [CrossRef]
[115] Park JH, Kim MH. Experimental investigation on comprehensive thermal-hydraulic performance of supercritical CO2 in a NACA 0020 airfoil fin printed circuit heat exchanger. Int J Heat Mass Transf 2024;220:124947. [CrossRef]
[116] Han Z, Cui X, Guo J, Zhang H, Zhou J, Cheng K, et al. Experimental and numerical studies on the thermal-hydraulic performance of a novel airfoil fins printed circuit heat exchanger. Int J Heat Mass Transf 2023;215:124655. [CrossRef]
[117] Chung S, Lee SW, Kim N, Shin SM, Kim MH, Jo H. Experimental study of printed-circuit heat exchangers with airfoil and straight channels for optimized recuperators in nitrogen Brayton cycle. Appl Therm Eng 2023;218:119100. [CrossRef]
[118] Li Z, Lu D, Wang Z, Cao Q. Analysis on flow and heat transfer performance of SCO2 in airfoil channels with different fin angles of attack. Energy 2023;282:128600. [CrossRef]
[119] Li Z, Lu D, Wang X, Cao Q. Analysis on the flow and heat transfer performance of SCO2 in airfoil channels with different structural parameters. Int J Heat Mass Transf 2024;219:124846. [CrossRef]
[120] Liu X, Zhao Z, Li C, Ding J, Pu X. Investigation of local flow and heat transfer of supercritical LNG in airfoil channels with different vortex generators using field synergy principle. Appl Therm Eng 2024;242:122424. [CrossRef]
[121] Wu J, Xiao J. Numerical study of crossed airfoil fins in a printed circuit heat exchanger. Appl Therm Eng 2023;230:120646. [CrossRef]
[122] Li Z, Lu D, Cao Q, Wang Y, Liu Y. Research on the enhanced heat transfer performance of SCO2 caused by vortex generators with different geometric dimensions in novel airfoil channels. Prog Nucl Energy 2024;169:105057. [CrossRef]
[123] Ke Z, Zhang Y. Heat transfer enhancement in a rectangular channel with flow-induced pitching, heaving or surging of an airfoil. Int Commun Heat Mass Transf 2023;142:106657. [CrossRef]
[124] Jin F, Chen D. Numerical study on flow distribution of supercritical CO2 in multiple channels of printed circuit heat exchanger. Appl Therm Eng 2023;234:121185. [CrossRef]
[125] Samykano M. Role of phase change materials in thermal energy storage: Potential, recent progress and technical challenges. Sustain Energy Technol Assess 2022;52:102234. [CrossRef]
[126] K Sunil, Muniamuthu S, Aandi M, Amirthalingam P, Muthuraja MA. Effect of charging and discharging process of PCM with paraffin and $Al_2O_3$ additive subjected to three point temperature locations. J Ecol Eng 2022;23:34–42. [CrossRef]
[127] Pignata A, Minuto FD, Lanzini A, Papurello D. A feasibility study of a tube bundle exchanger with phase change materials: A case study. J Build Eng 2023;78:107622. [CrossRef]
[128] Arqam M, Raffa LS, Clemon LM, Islam MS, Ryall M, Bennett NS. Numerical and experimental investigation of a phase change material radial fin heat sink for electronics cooling. J Energy Storage 2024;98:113113. [CrossRef]
[129] Taghavi M, Poikelispää M, Agrawal V, Syrjälä S, Joronen T. Numerical investigation of a plate heat

exchanger thermal energy storage system with phase change material. J Energy Storage 2023;61:106785. [CrossRef]

[130] Abdulateef AM, Abdulateef J, Sopian K, Mat S, Ibrahim A. Optimal fin parameters used for enhancing the melting and solidification of phase-change material in a heat exchanger unit. Case Stud Therm Eng 2019;14:100487. [CrossRef]

[131] Mastani Joybari M, Selvnes H, Vingelsgård E, Sevault A, Hafner A. Parametric study of low-temperature thermal energy storage using carbon dioxide as the phase change material in pillow plate heat exchangers. Appl Therm Eng 2023;221:119796. [CrossRef]

[132] Khader MA, Ghavami M, Al-Zaili J, Sayma AI. Residential Micro-CHP system with integrated phase change material thermal energy storage. Energy 2024;300:131606. [CrossRef]

[133] Asgari M, Javidan M, Nozari M, Asgari A, Ganji DD. Simulation of solidification process of phase change materials in a heat exchanger using branch-shaped fins. Case Stud Therm Eng 2021;25:100835. [CrossRef]

[134] Yazdani MR, Lagerström A, Vuorinen V. Simultaneous effect of biochar-additive and lightweight heat exchanger on phase change material for low-grade thermal energy storage. J Energy Storage 2022;55:105478. [CrossRef]

[135] Zhang J, Cao Z, Huang S, Huang X, Han Y, Wen C, et al. Solidification performance improvement of phase change materials for latent heat thermal energy storage using novel branch-structured fins and nanoparticles. Appl Energy 2023;342:121158. [CrossRef]

[136] Fan M, Jiang H, Wang J, Li H, Jin F, Kong X. Study and optimization on heat storage and release characteristics of a cascaded sensible-latent heat composite energy storage heat sink. Energy Built Environ 2025;6:161−172. [CrossRef]

[137] Safari V, Kamkari B, Gharbi A. Wedge-shaped fins to enhance thermal performance of shell and tube heat exchangers containing phase change material: An experimental study. Therm Sci Eng Prog 2024;49:102474. [CrossRef]